CHEMISTRY OF MATERIALS

REVIEW

pubs.acs.org/cm

Electron Transfer Dynamics in Dye-Sensitized Solar Cells

Andrea Listorti, Brian O'Regan,* and James R Durrant*

Centre for Plastic Electronics, Department of Chemistry, Imperial College London, London SW7 2AZ, United Kingdom

ABSTRACT: In this review, we address the materials design parameters that control the processes of charge separation, and thereby device efficiency, in dye-sensitized photoelectrochemical solar cells. The review starts with an overview of the structure, energetics and kinetics of dye-sensitized solar cells. It then goes on to consider in more detail the parameters determining the efficiency of the two primary charge separation steps in these devices: electron injection from the dye excited state into the metal oxide electrode, and regeneration of the dye ground state by the redox electrolyte. We consider the kinetic competition between these desired charge separation steps and the undesired loss pathways of excited state decay to ground and electron recombination with dye cations. The review avoids detailed mathematical and spectroscopic discussion, but rather tries to summarize the key conclusions relevant to materials design. A recurring theme of the review is the energy cost of achieving charge separation, and how this limits device performance. A further factor addressed in this review is real as opposed to ideal materials behavior, including, for example, consideration of the implications of empirical observations of an exponential density of acceptor states in the metal oxide, as well as identification of unresolved issues in our current understanding.

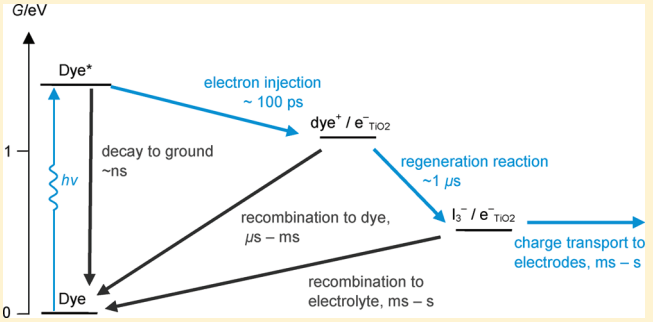

KEYWORDS: dye-sensitized solar cell, electron transfer, photoelectrochemistry, electron injection, mesoporous

1. INTRODUCTION

Dye-Sensitized solar cells (DSSCs) are one of the emerging solar technologies that offers the potential to reduce the cost of photovoltaic electricity generation. Over the last 20 years there has been extensive academic and, increasingly, commercial interest in this technology. This was initiated by the report by O'Regan and Grätzel in 1991 of an efficient photovoltaic device based on a mesoporous, nanocrystalline titania electrode sensitized to visible light by the adsorption of a ruthenium bipyridyl dye in the presence of an iodide/iodine redox electrolyte.[1] Over this period, there has been great progress in the materials composition of such devices not only to enhance device efficiency, but also to improve stability and processability and to reduce production costs. These materials advances have been reviewed extensively elsewhere.[2−8] In parallel with these materials advances, great progress has been made at understanding the science of the processes underlying device performance.[9−13] In this review, we focus upon relating these two areas, considering how advances in fundamental understanding of function can help guide materials and device development.

The primary energy conversion process in dye-sensitized solar cells is a photoinduced charge separation at the metal oxide/dye/electrolyte interface. Initial studies of this charge separation were largely based upon model system studies such as dye sensitized metal oxide films in the absence of redox electrolyte or solar irradiation. Such studies have allowed us to develop some understanding of the parameters determining these charge separation kinetics, as we and others have reviewed elsewhere.[3,11,12,14−17] In parallel with these studies, time and frequency domain photoelectochemical analyses have made great progress in developing a detailed picture of overall device function,[18−24] although such studies lack the time resolution to analyze the charge separation processes in detail. It is only relatively recently that transient kinetic studies have focused upon the measurement of charge separation kinetics under conditions relevant to device operation, and tried to correlate these kinetics directly with photovoltaic device performance. In this review, we focus specifically upon this issue. We start with an overview of device function, with a particular focus on charge separation. We then go on to consider in more detail the two key kinetic competitions which can limit the efficiency of charge separation and thereby device performance: electron injection versus excited state decay to ground and dye regeneration versus electron recombination with dye cations. Throughout our review, we consider the impact of materials and device design upon these kinetics, and furthermore the lessons which can be learned from such kinetic studies for future materials optimization.

2. OVERVIEW OF DYE-SENSITIZED SOLAR CELL FUNCTION

2.1. Device Composition. Figure 1 is a schematic of the components of a DSSC. At the heart of the system is a mesoporous oxide layer composed of nanometre-sized particles that have been sintered together to allow electronic conduction to take place. The material of choice has been TiO_2 (anatase) although alternative wide-gap oxides such as ZnO, SnO_2, and Nb_2O_5 have also been investigated.[25−34] Attached to the surface of the

Received: March 4, 2011
Revised: April 20, 2011
Published: May 09, 2011

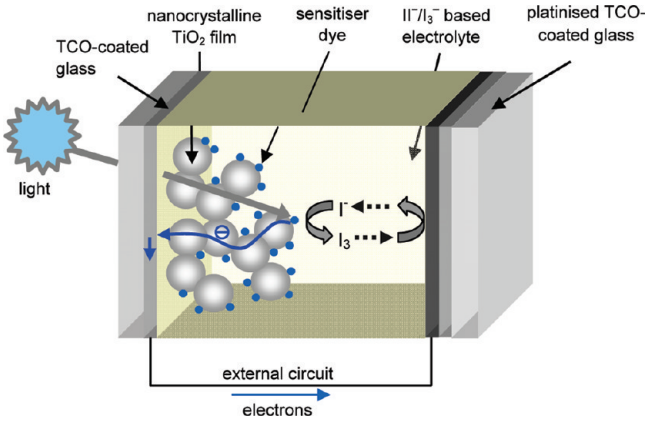

Figure 1. Schematic of a liquid electrolyte dye-sensitized solar cell. Photoexcitation of the sensitizer dye is followed by electron injection into the conduction band of the mesoporous oxide semiconductor, and electron transport through the metal oxide film to the TCO-coated glass working electrode. The dye molecule is regenerated by the redox system, which is itself regenerated at the platinised counter electrode by electrons passed through the external circuit.

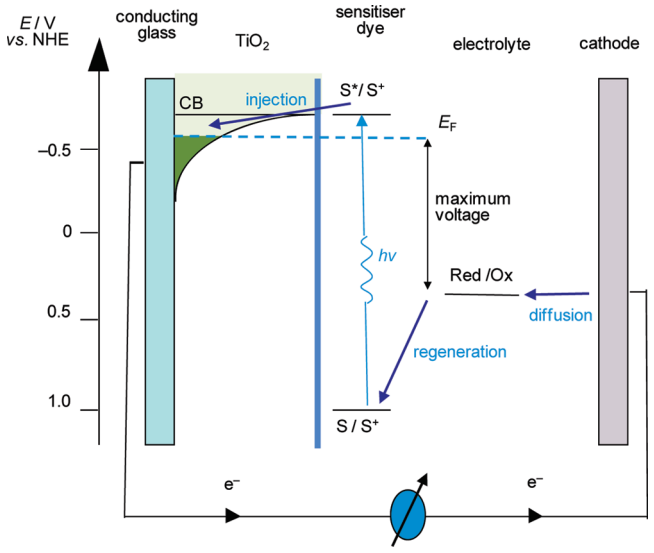

Figure 2. Energetics of operation of DSSCs. The primary free-energy losses are associated with electron injection from the excited sensitizer into the TiO_2 conduction band and regeneration of the dye by the redox couple. The voltage output of the device is approximately given by the splitting between the TiO_2 Fermi level (dashed line) and the chemical potential of the redox electrolyte. We note that in this typical diagram the conduction band energy is a one-electron energy, not a free energy. We explain the placement of the conduction band edge approximately isoenergetic to the dye excited state in the text.

nanocrystalline film is a monolayer of a sensitizer dye. The most widely studied sensitizer dye is the Ru-bipyridyl dye **N719**, which is the ditetrabutyl-ammonium salt of $RuL_2(NCS)_2$ where L = 4, 4′-dicarboxy-2,2′-bipyridine. Photoexcitation of the sensitizer dye results in the injection of an electron into the conduction band of the oxide, generating the oxidized form of the dye (referred to herein as S^+ or D^+, although we note that the oxidized dye does not always have a formal positive charge). We note that to save space we will use the term "conduction band" to refer generically to electron acceptor states in the oxide. (These acceptor states may be an extension of a bulk conduction band to the surface, with a parabolic density of states (DOS) at the conduction band edge. Alternatively, these states may be localized or extended surface states whose DOS in the energetic region of the injection may have other shapes, such as an exponential form as discussed below). After electron injection, the ground state of the dye is subsequently restored by electron donation from the electrolyte; this step is often referred to as the regeneration reaction. The electrolyte is usually an iodide/triiodide redox couple dissolved in a liquid organic solvent, although attention is increasingly focusing on alternatives for the solvent, including ionic liquids, gelled electrolytes, polymer electrolytes, and water-based electrolytes.[35−43]

The regeneration of the sensitizer by iodide intercepts the recapture of the injected electron by the oxidized dye. The iodide is in turn regenerated by the reduction of triiodide at the counter electrode, with the electrical circuit being completed via electron migration through the external load. The high surface area of the mesoporous metal oxide film is critical to efficient device performance as it allows strong absorption of solar irradiation to be achieved by only a monolayer of adsorbed sensitizer dye. Whereas a dye monolayer absorbed on a flat interface exhibits only negligible light absorption (the optical absorption cross-sectional areas for molecular dyes being typically 2−3 orders of magnitude smaller than their physical cross sections), the use of a mesoporous film dramatically enhances the interfacial surface area over the geometric surface area, by up to a 1000-fold for a 10 μm thick film, leading to high visible-light absorbance from the many successive monolayers of adsorbed dye in the optical path. Another advantage of the use of a dye monolayer is that there is no requirement for exciton diffusion to the dye/metal oxide interface; moreover, the nonradiative quenching of excited states often associated with thicker molecular films is avoided. The high surface area of such mesoporous films does, however, have a significant downside, as it also enhances interfacial charge-recombination losses, a topic we return to in more detail below.

There are extensive efforts to develop alternative material components for DSSCs to improve device efficiency, stability, cost and/or processability. These include alternative metal oxides and metal oxide nanostructures (e.g., nanowires),[26−28] alternative sensitizer dyes including in particular organic rather than inorganic co-ordination dyes;[4,25,44−47] alternative electrolyte components including alternative solvents, redox couples, and additives;[6,48−53] and replacing the redox electrolyte with a solid-state hole conductor, which may be either inorganic.[54,55] or organic.[56] Devices efficiencies for such solid-state DSSCs are as yet limited to ~5%,[2,57] in contrast to efficiencies of over 11% achieved for the more widely studied redox electrolyte-based DSSCs.[58] In all such materials changes, there is an increasing appreciation that changing any one materials component of the device is likely to impact upon more than one of the key functional processes determining device performance, underlining the importance of undertaking such materials changes in parallel with detailed functional studies.

2.2. Energetics of Operation. Charge separation in DSSCs can be regarded as a two-step redox cascade, resulting in the injection of electrons into the TiO_2 electrode and the subsequent oxidation of the redox electrolyte, with the latter also resulting in regeneration of the dye ground state. Figure 2 shows typical values for the interfacial energetics in a DSSC. Both the injection and regeneration charge-separation reactions are thermodynamically downhill. The kinetics, energetics and quantum efficiency of injection and regeneration will be reviewed in detail in sections 4 and 5 of this article.

dx.doi.org/10.1021/cm200651e |Chem. Mater. 2011, 23, 3381–3399

Following charge separation, charge collection from the device requires transport of the photogenerated charges to their respective electrodes. For an efficient DSSC under AM1.5 solar irradiance, these charge fluxes are of the order of 20 mA cm^{-2}. The high ionic concentrations in the device effectively screen out any macroscopic electric fields, thereby removing any significant drift component of these transport processes. The transport of both electrons and redox ions are therefore both primarily driven by diffusion processes resulting from concentration gradients. Under optimum conditions (e.g., good TiO_2 nanoparticle interconnections and a low-viscosity electrolyte), these charge-transport processes (electrons toward the FTO working electrode, triiodide toward the counter electrode) can be efficiently driven with only modest concentration gradients, and therefore only small free energy losses. At the counter electrode, the triiodide is rereduced back to iodide, the platinum catalyst enabling this reaction to proceed with minimal overpotential. A similarly ohmic contact can be achieved at the TiO_2/FTO interface. It is thus apparent that the energetics at the TiO_2/dye/electrolyte interface are of primary importance in determining the overall device output.

Power output from the DSSC requires not only efficient charge separation and collection by the electrodes, resulting in a photocurrent, but also the generation of a photovoltage, corresponding to a free energy difference between the working and counter electrodes. In the dark at equilibrium, the Fermi energy of the TiO_2 electrode (corresponding to the free energy of electrons in this film after thermalisation) equilibrates with the midpoint potential of the redox couple, resulting in zero output voltage. Under these conditions, the TiO_2 Fermi level lies deep within the band gap of the semiconductor, and the film is effectively insulating, with a negligible electron density in the TiO_2 conduction band. Photoexcitation results in electron injection into the TiO_2 conduction band and concomitant hole injection into (oxidation of) the redox electrolyte. The high concentrations of oxidized and reduced redox couple present in the electrolyte mean that this electrolyte photooxidation process does not result in a significant change in chemical potential of the electrolyte, which remains effectively fixed at its dark, resting value. In contrast, electron injection into the TiO_2 conduction band results in a dramatic increase in electron density (from the order of 1×10^{13} cm^{-3} to 1×10^{18} cm^{-3}), raising the TiO_2 Fermi level toward the conduction-band edge. This shift of the TiO_2 Fermi level under irradiation corresponds to an increase in the stored free energy of injected electrons and is responsible for the generation of the photovoltage in the external circuit.

The midpoint potential of the redox couple is given by the Nernst equation, and is therefore dependent on the relative concentrations of iodide and iodine. The concentrations of these species required for efficient device function are in turn constrained by kinetic requirements of dye regeneration at the working electrode, and iodide regeneration at the counter electrode, as discussed below. Typical concentrations of these species are in the range 0.1−0.7 M iodide and 10−200 mM iodine, constraining the midpoint potential of this electrolyte to ~0.3 V vs. NHE. It should furthermore be noted that in the presence of excess iodide, the iodine is primarily present in the form I_3^-, resulting in this electrolyte often being referred to as an iodide/triiodide redox couple.

Determining the energetics of the TiO_2 conduction band is more complex. As with most oxides, the surface of TiO_2 may be more or less protonated depending on the proton activity of the surrounding medium. The resultant changes in surface charge cause the surface potential to exhibit a Nernstian dependence on

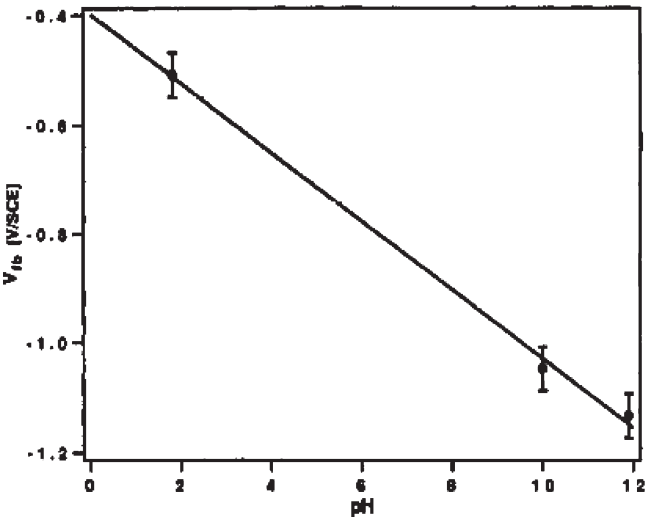

Figure 3. Flatband potential of a mesoporous TiO_2 film as a function of the pH value of the aqueous solution. Reproduced with permission from ref 60. Copyright 1992 American Chemical Society.

effective pH, shifting by 60 mV per pH unit when in water,[59,60] as illustrated in Figure 3. In bulk metal oxides, surface charge can be associated with significant bending of the conduction and valence bands adjacent to the surface. However, in the mesoporous TiO_2 films employed in DSSCs, the nanoparticles are too small to support significant band bending under depletion. As a consequence, the whole conduction band of such mesoporous films shifts with the surface potential. DSSCs typically employ organic rather than aqueous electrolytes, complicating quantification of the effective pH. Nevertheless studies in organic solvents have demonstrated shifts of the conduction band of mesoporous TiO_2 films of up to 1 V depending on the concentration of potential-determining ions (primarily small cations such as protons or lithium cations) in the electrolyte.[61] For this reason, the concentration of such potential-determining ions in the electrolyte plays a key role in determining the energetics of the dye-sensitized interface, and thereby device performance. Additives added to the electrolyte to determine such energetics include Li^+, guanadinium ions, N-methylbenzimidazole and *t*-butyl pyridine (the latter two function as bases). Further influence on these interfacial energetics can be achieved by variation of the extent of protonation of the sensitizer dye.[62]

The choice of sensitizer dye energetics is essential to achieve suitable matching to the metal oxide and redox couple. The excited-state oxidation potential ($E_{ox}^* = E_m(D^+/D^*)$) must be sufficiently negative to achieve efficient electron injection into the TiO_2 conduction band, while the ground-state oxidation potential must be sufficiently positive to oxidize the redox couple. The redox properties of adsorbed sensitizer dyes may differ significantly from those measured in solution, mainly due to the high surface-charge densities and dipoles present at this interface.[63] Notwithstanding this, typical dye ground state oxidation potentials empirically found to be compatible with efficient device function are $E_m(D^+/D) > 0.6$ V vs. NHE.

2.3. Kinetics of Operation. We present in this section an overview of electron transfer dynamics in DSSCs. These dynamics are then considered in more detail in sections 4 and 5. Figure 4 illustrates a photochemical view of the function of a DSSC, illustrating the sequence of electron transfer and charge-transport processes which result in photovoltaic device function.

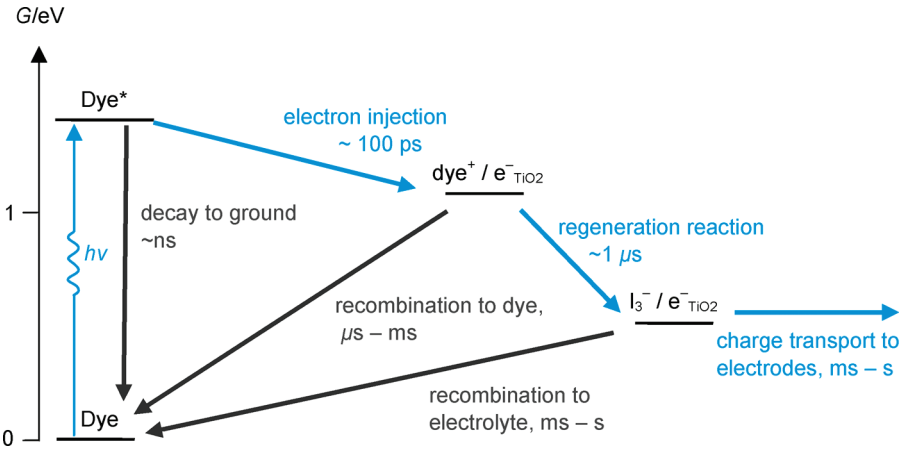

Figure 4. State diagram representation of the kinetics of DSSC function. Forward processes of light absorption, electron injection, dye regeneration, and charge transport are indicated by blue arrows. The competing loss pathways of excited-state decay to ground and electron recombination with dye cations and oxidized redox couple are shown in gray. The vertical scale corresponds to the free energy stored in the charge-separated states. Note the free energy of injected electrons is determined by the Fermi level of the TiO_2; the figure is drawn assuming a TiO_2 Fermi level 0.6 V above the chemical potential of the redox electrolyte (corresponding to a cell voltage of 0.5−0.6 V, close to the maximum power point of typical DSSCs). Adpated with permission from ref 3. Copyright 2008 Imperial College Press.

In addition to the forward electron transfer and transport processes, this figure also illustrates several competing loss pathways, shown as black arrows. These loss pathways include decay of the dye excited state to ground, and charge recombination of injected electrons with dye cations and with the redox couple. Each charge-transfer step results in an increased spatial separation of electrons and holes, increasing the lifetime of the charge-separated state, but at the expense of reducing the free energy stored in this state. This functionality exhibits a close parallel to function of photosynthetic reaction centers. As in natural photosynthesis, kinetic competitions between the various forward and loss pathways are critical to determining the quantum efficiencies of charge separation and collection, and are therefore key factors determining energy conversion efficiency.

It is important to appreciate that the efficiency of electron injection in DSSCs depends not upon the absolute kinetics of electron injection, but rather on the magnitude of these injection kinetics relative to excited-state decay to ground. Typical rates of excited-state decay vary substantially between sensitizer dyes from picoseconds to nanoseconds—with consequently very different requirements on the kinetics of electron injection necessary for efficient device function. A further consideration is the potential for electron injection not only from dye singlet but also triplet excited states. Such triplet states are typically formed by intersystem crossing from the singlet excited state, and are longer lived, but less energetic, than the corresponding singlet state. For inorganic coordination dyes, such as ruthenium bipyridine analogues, intersystem crossing from the singlet to triplet state can be as fast as $1 \times 10^{13}\ s^{-1}$. In general, singlet state lifetimes range from 1×10^{-13} to 1×10^{-9} s, and triplet state lifetimes range from nanoseconds to milliseconds (dependent on the solvent/electrolyte environment). As such, consideration of the efficiency of electron injection requires careful consideration of not only the rate of electron injection, but also the kinetics of excited-state decay.

Considering the rate of electron injection from the dye excited state, this depends upon the electronic coupling between the dye LUMO orbital and accepting states in the TiO_2, and on the number density of these states at the surface near the dye. In model system studies of dye-sensitized metal oxide films, electron injection rates of $>1 \times 10^{12}\ s^{-1}$ have been reported for a range of sensitizer dyes, consistent with efficient electron injection.[11,16,64] However, it should be noted that fast electron injection dynamics require both strong electronic coupling of the dye LUMO orbital to the metal oxide conduction-band states, and a large density of states in the TiO_2 energetically accessible from the dye excited state. Following electron injection, injected electrons undergo rapid thermalisation down to the electron Fermi level of the electrode. This thermalisation process constitutes a loss in free energy and is therefore a limitation on device efficiency, as we discuss further below. The electron injection dynamics are dependent on the energy of the TiO_2 conduction band relative to the dye excited state oxidation potential. This is turn depends upon the concentration of potential-determining ions (e.g., Li^+) in the electrolyte. Omission of acidic ions from the electrolyte can result in a high energy conduction band. The resulting lower density of accessible acceptor states gives slower injection, and can reduce the quantum yield of charge injection, and thereby lower device photocurrent.[15,65−69]

Efficient dye regeneration requires that the rate of rereduction of the dye cation by the redox couple exceeds that of charge recombination of injected electrons with these dye cations. This recombination reaction has been shown to be strongly dependent on the electron density in the TiO_2 electrode (or film Fermi level) and therefore light intensity and cell voltage, accelerating by at least an order of magnitude between short-circuit and open-circuit conditions.[64] It is furthermore dependent on the spatial separation of the dye cation (HOMO) orbital from the metal oxide surface, with the rate constant decaying exponentially with distance, consistent with electron tunneling theory.[70] The regeneration reaction is dependent on the iodide concentration, electrolyte viscosity and dye structure. For the **N719** sensitizer dye, and employing a low-viscosity electrolyte such as acetonitrile, the regeneration reaction has a half-time of ~1 μs, sufficiently fast to compete effectively with the competing recombination reaction and ensuring that the regeneration reaction can be achieved with unity quantum efficiency.[31]

Efficient charge collection by the external circuit requires the time constant for electron transport to the collection electrode to be faster than charge recombination of injected electrons with

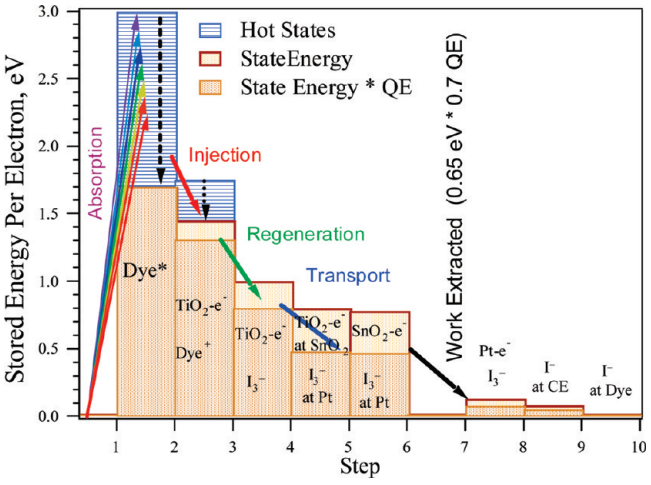

Figure 5. State energy diagram of a typical DSSC under one sun illumination at the maximum power point (MPP). Energy and quantum efficiency values are approximate and will change depending on dye and electrolyte composition. Reproduced with permission from ref 10. Copyright 2009 American Chemical Society.

the redox couple. Electron transport is a diffusive process, strongly influenced by electron trapping in localized sub-bandgap states, resulting in the dynamics being strongly dependent on position of the TiO_2 electron Fermi level: raising the Fermi level toward the conduction-band edge resulting in increased trap filling. There have been several recent analyses of charge collection in DSSCs, including detailed consideration of the kinetics and energetics of these processes.[18,19,71] These processes will not be considered further in this review, except where relevant to our consideration of the primary charge separation steps of electron injection and dye regeneration.

The kinetics of charge separation and collection are related to the energetic losses involved in each of the functional processes in DSSCs, as we have discussed recently.[10] Ultimately, these energetic losses are the cause of the device output voltage being significantly less than its optical bandgap—with typical device voltages at maximum power output being in the range 0.6—0.75 V, less than half the absorption onset of typical sensitizer dyes. These energy losses depend not only upon the materials composition of the cell, but also upon the device operating condition. We consider the balance between kinetics and energetics, and its impact upon overall device performance, in more detail in sections 4 and 5 of this review.

2.4. Energetic Losses in DSSCs. Figure 5 illustrates the energetics of DSSC operation for a typical device achieving an overall power conversion efficiency of ~9.5%. The bold bars are the state energies given by the electron and hole chemical potentials after each step. The lighter bars (and shaded areas) are this same state energy, reduced by the quantum efficiency (QE) losses up to that point (State Energy × QE), determined specifically for the maximum power point (MPP) situation of this typical moderately efficient DSSC. The differences between the successive shaded bars show how much each step costs in a real cell under operation. Also shown (in blue) is the excess energy generated by the absorption of photons at shorter wavelengths than the optical band gap, with this excess energy being lost to excited state thermalisation processes. Large steps down on this graph indicate where research breakthroughs might cause large increases in cell efficiency. For the case illustrated, the MPP is assumed to correspond to a device voltage of 0.65 V and a photon to electron quantum efficiency of 0.7, yielding 0.65 × 0.7 = 0.46 eV of work extracted per absorbed photon. For a typical DSSC with the **N719** dye, this yields a device efficiency of ~9.5% under AM1.5 irradiation. It is apparent that each functional step is associated with a free energy loss driving this step. Minimising these free energy losses, while maintaining high quantum efficiencies, is critical to achieving advances in device efficiency.

3. CHALLENGES IN TRANSIENT KINETIC STUDIES OF DSSCS

Most studies of the electron transfer dynamics relating to DSSCs have been undertaken on model systems. The use of such model systems has largely been motivated by the desire to study a specific process in isolation. For example, studies of electron recombination to photooxidized dyes (D^+) have typically been undertaken in the absence of a redox electrolyte, so that the observed decay dynamics of the D^+ can be assigned directly to this recombination reaction without having to consider contributions to the dynamics from rereduction of the D^+ by the redox electrolyte. A further motivation for such model system studies is that they are technically often easier. For example, the most widely used experimental technique to study electron injection is ultrafast pump/probe spectroscopy. Such measurements typically use relatively high pulse intensities and repetition rates to achieve adequate signal-to-noise — resulting in relatively high overall light fluences which can exceed solar fluence by 10—100 fold. In complete DSSCs, where the lifetime of the final charge separated state ($I_3^-/e^-_{TiO_2}$) is on the milliseconds to seconds time scale, these high light fluences can result in significant charge accumulation in the device, potentially complicating the interpretation of such experiments. As such, pump/probe studies of electron injection in DSSC have rotated or translated the cell at sufficient speed to minimize this charge accumulation, greatly complicating the execution of such experiments.[15—17] This charge accumulation issue is largely avoided by studying dye sensitized films without redox couple, as the shorter lifetime of the charge separated state (in this case $dye^{+\cdot}/e^-_{TiO2}$) greatly reduces charge accumulation. Because of these limitations, very few pump/probe kinetic studies of electron injection to date have included a regenerating redox couple in the sample.[68,69,72—75] As an alternative approach, it has recently been shown that time correlated single photon counting can be employed to study the kinetics of electron injection in complete devices.[76—78] This technique, although more limited in time resolution, employs much lower excitation densities, thereby avoiding the charge accumulation limitations associated with more widely used pump/probe studies.

The importance of undertaking kinetic studies under conditions as closely corresponding to complete devices can be appreciated by consideration of the chemical composition of the system. Figure 6 shows to scale the composition of a pore of this film in the presence of a typical electrolyte employed in a DSSC.[10] This schematic neglects electrolyte molecular interactions or surface binding, which is likely to modulate further the chemical composition of these pores. Note that a typical 1 cm^2 cell has 2 μL of electrolyte and a TiO_2 surface area on the order of 1000 cm^2. A strong adsorption to the surface could therefore fully deplete the electrolyte of a component initially present at ≤0.1 M. It is apparent that the pore volume is chemically complex, with a wide range of molecular and surface interactions which may modulate not only the relevant energetics but also the interface

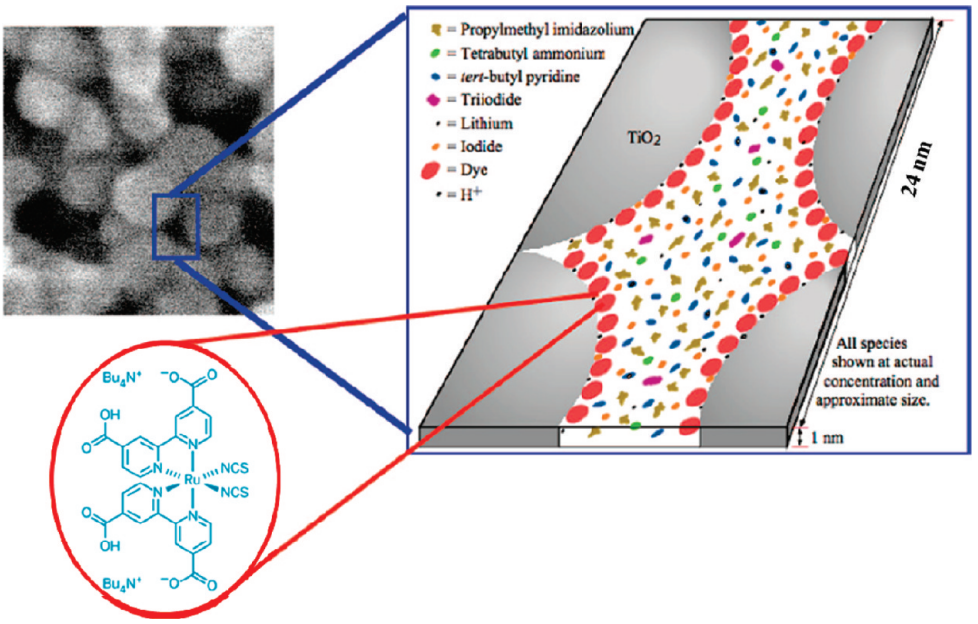

Figure 6. Schematic of the chemical composition of a typical pore in a complete DSSC filled with redox electrolyte. All components are drawn approximately to scale, neglecting molecular interactions. Also shown is a HRSEM image of such a pore, and the molecular structure of the **N719** sensitizer dye. This illustration neglects intermolecular complexation which is likely to further complicate the chemical composition of the pores. Reproduced with permission from ref 10. Copyright 2009 American Chemical Society.

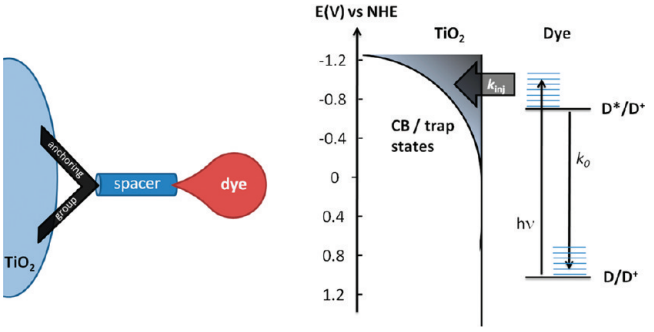

Figure 7. Schematic representation of the molecule-semiconductor nanoparticle interface and the energetic/kinetics scheme determining the injection yield.

structure (and therefore electronic coupling) and local concentrations of active species (e.g.: iodide ions). As such, considerable caution should be taken when relating model system studies directly to device performance.

A further consideration when relating kinetic studies to device operation is the impact of device operating conditions. As we have discussed above, solar irradiation can be expected to increase significantly the density of electrons in the TiO_2, impacting directly upon the observed interfacial energetics and kinetics. In addition, solar irradiation results in the development of concentration gradients in the electrolyte.[79,80] This can modulate the concentration of species in the film pores, particularly in cases where the electrolyte employed is relatively viscous (as often used where device stability is a priority). Finally, solar irradiation can be expected to change the electrostatic charge environment of the interface, as has recently been reported from observation of Stark effects in transient kinetic studies.[81] As such, again caution must be taken relating transient measurements which typically collected in the dark (apart from the excitation/measurement light) with device behavior in the light under operation.

4. PRIMARY CHARGE SEPARATION: ELECTRON INJECTION FROM THE DYE EXCITED STATE

4.1. Injection Kinetics in Dye-Sensitized Metal Oxide Film Studies. Efficient electron injection requires that electron injection is fast relative to excited state decay to ground. Kinetic competition between these two processes is critical to determining the quantum efficiency of charge photogeneration in DSSCs. In this section we focus upon the rate constant for electron injection, k_{inj}. Figure 7 shows a schematic of photoinduced ET at the molecule-semiconductor interface. In general, the system can be described as a donor-bridge-acceptor complex with a molecule (electron donor) anchored to the semiconductor nanoparticle surface (electron acceptor) through a molecular anchoring/spacer group (bridge). Once the electron is injected into the semiconductor, it undergoes thermal relaxation and trapping in intraband states. The high dielectric constant of the TiO_2, coupled with the high ionic strength of the electrolyte, is generally thought to result in negligible Coulombic interactions between the sensitizer dye cation and the injected electron. As such, there is typically little evidence for the formation of interfacial charge transfer states, nor for significant geminate recombination losses in DSSCs.[82,83] We note this situation appears to be significantly different from that observed in organic polymer/fullerene solar cells where, because of the lower organic film dielectric constant, geminate recombination of interfacial charge transfer states is thought to be a key loss pathway.[84]

The theoretical description of excited-state electron injection at solid/liquid interfaces into wide-bandgap semiconductors was developed by Marcus and Gerischer in the late '60s.[85−87] Recent advances in theoretical analyses of this process in DSSCs have been reviewed recently elsewhere.[88] The electron injection rate

may be expressed as the sum of ET rates to all possible accepting states in the semiconductor[89]

$$k_{inj} = A\int V^2(1-f(E,E_F))\rho(E)\exp\left(\frac{-(E-E_{ox}^*+\lambda)^2}{4\pi\lambda k_B T}\right)dE \quad (1)$$

where E is the absolute energy relative to NHE of the semiconductor acceptor state, E_{ox}^* is the redox potential of dye excited state; $\rho(E)$ is the density of semiconductor acceptor states at energy E relative to NHE; V is the average electronic coupling between the dye excited state and different states in the semiconductor at the same energy E; $f(E, E_F)$ is the Fermi occupancy factor for each semiconductor acceptor state, as determined from the semiconductor electron Fermi level E_F; and λ is the total reorganization energy for electron injection. The dye excited state oxidation potential is typically estimated from $E_{ox}^* = E(D/D^+) - E_{00}$ where $E(D/D^+)$ is the ground state oxidation potential and E_{00} is the excited state energy estimated from the midpoint of the dye absorption and emission spectra. A consequence of the exponential term in eq 1 is that electron injection occurs optimally to acceptor states λ below the dye excited state oxidation potential. We discuss below how each of these factors can impact upon the kinetics of electron injection.

We consider first the impact of the semiconductor acceptor density of states $\rho(E)$ in determining the rate constant for electron injection. Following eq 1, the primary consideration is the energetics and shape of $\rho(E)$ relative to the dye excited state oxidation potential E_{ox}^*. Many literature studies are based upon assuming $\rho(E)$ corresponds to an ideal semiconductor conduction band density of states, increasing quadratically above a well-defined conduction band edge ($\rho(E) \propto (E - E_{CBE})^2$), supported by model system studies such as X-ray photoelectron spectroscopies taken upon metal oxide films under high vacuum.[11,90−92] In papers about electron injection into TiO_2, it is typical to draw this conduction band edge near -0.5 V vs NHE.[12,66,93,94] This tradition probably stems from earlier studies in acidic water and organic electrolyte without base, where the conduction band was measured to be at this level.[83,95] This conduction band edge is approximately 200 mV below the excited state oxidation potential for the widely used N719 sensitizer, typically estimated at approximately −0.7 V vs NHE, providing an apparent energy offset to drive ultrafast electron injection. However we note these studies employed relatively acidic electrolytes (corresponding to DSSCs with open circuit voltage's near 0.5 V). Less acidic electrolytes, such as those employed in most current device studies, typically yield much higher open circuit voltages, typically ≥0.8 V. Consistent with these higher voltages, recent modeling of transport and recombination in DSSCs employing such electrolytes typically indicate TiO_2 conduction band edges (or mobility edges) near −0.7 V vs NHE (corresponding to −1 V vs I^-/I_3^-).[23,96−99] Such analyses would place the N719 excited state approximately energetic with the TiO_2 conduction band edge.

A key concern for the analyses of electron injection assuming a well-defined, parabolic density of states, as discussed in the preceding paragraph, is that most experimental measurements of $\rho(E)$ in the presence of electrolyte observe not a parabolic density of states with a well-defined conduction band edge, but rather an exponentially increasing density of states, $\rho(E) \propto \exp(E/E_0)$, with E_0 in the range 80−100 meV,[23,98,100,101] as illustrated in Figure 7. Efforts to find the potential at which this exponential density of states transforms to a parabolic conduction band have not been successful.[102,103] This exponential density of states has typically been assigned to a tail of relatively localized intraband states, corresponding to electron poor Ti^{4+} sites which are subject to reduction to Ti^{3+} at a lower potential than the conduction band (e.g., an oxygen vacancy, or a more electronegative impurity on the oxygen site). We note that this exponentially increasing density of states may also in part originate from an inhomogeneous distribution of conduction band edge energies, resulting for example from differences in nanoparticle crystal surface or charge.[82] Integration of this observed exponential tail of localized states up to the estimated conduction band energy at −0.7 V yields approximately 5×10^{19} states/cm^3 of TiO_2, corresponding to approximately 200 localized states per typical nanoparticle the average particle, in good agreement with modeling studies of trap limited recombination.[104,105] A key, and currently unresolved question, for electron injection in DSSC is the extent to which electron injection can proceed directly into these localized states, as we discuss further below.

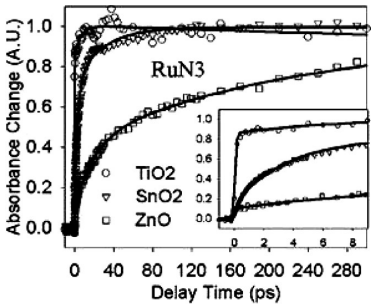

Figure 8. Comparison of electron injection rates to TiO_2, ZnO, and SnO_2 from N3 (the fully protonated analogue of N719). For all samples, the dye was excited at 400 nm and absorption of injected electrons probed at 5 μm. Reproduced with permission from ref 66.

If injection proceeds from excited dyes into an exponential band of acceptor states, injection rates should have a similar exponential relation to changes in the relative energetics of the dye and acceptor states. Several model systems studies of dye sensitized metal oxide films have addressed the dependence of the rate of electron injection upon $\rho(E)$, including both comparisons of different metal oxides and studies as a function of ion concentration in the electrolyte.[65−68] For example, a 7-fold increase in injection dynamics was observed following addition of 0.1 M Li^+ ions to the electrolyte, consistent with the expected change in the energetics of $\rho(E)$ with concentration of this potential determining ion.[69] A similar pH dependence of electron injection has also been reported by Lian et al. in both aqueous and organic solvents.[106,107] Similarly differences in electron injection rates into TiO_2, SnO_2 and ZnO electrodes have been shown to be consistent with differences in the densities of acceptor states between these metal oxides, assigned in part to differences in electron effective mass between these materials, Figure 8.[16]

A second factor determining the energetics, and therefore the rate, of electron injection is the dye excited state oxidation potential E_{ox}^*. Following eq 1, and assuming injection into an exponential increasing density of acceptor states with $E_0 \sim$ 100 meV, a 100 meV increase in dye excited state energy can be expected to increase the density of acceptor states, and therefore k_{inj}, by exp(100/100) − approximately a three-fold increase.

dx.doi.org/10.1021/cm200651e |Chem. Mater. 2011, 23, 3381–3399

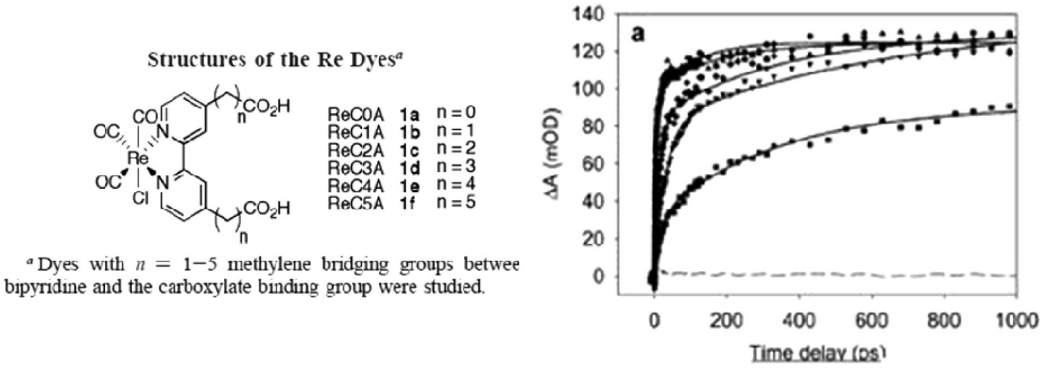

Figure 9. Injected electron traces probing at 2120−2150 cm^{-1} for ReC1A (●), ReC2A (▲), ReC3A (♦), ReC4A (▼), and ReC5A (■), all on SnO_2 film at pH 2. In this figure, the electron injection is followed observing the rise of the IR signal attributed to the electrons absorption in the SnO_2. The solid lines are two-exponential fits to the data. The dashed line is the signal from an unsensitized SnO_2 film, which has been already been subtracted from the other traces. Reproduced with permission from ref 122. Copyright 2003 American Chemical Society.

Several studies have reported variations in electron injection rate constants as a function of dye excited state energy approximately consistent with this dependence.[66,77,78,93,108−111] This energetic dependence is particularly important for the development of sensitizer dyes with red-shifted absorption spectra (critical for enhancing the photocurrent densities in DSSCs[9,10]), as in general the lower optical bandgap (E_{00}) will lower the dye excited state energy and therefore slow down electron injection.[112]

We note that, on ultrafast time scales, the energy of the dye excited state may be dependent upon the wavelength of photon absorbed. The absorption of photons with energies greater than the optical bandgap (e.g.: blue photons) initially generates thermally hot excited states (as illustrated in Figure 5). Indeed several model system studies have reported faster electron injection when employing such blue-shifted optical excitation.[66,73,74,113−115] However, such "hot" electron injection is probably only observed under conditions where the dye excited state is energetically high above the conduction band edge (e.g., in the presence of a high concentration of protons or lithium ions), and is therefore likely to be relatively unimportant in optimized DSSCs designs reported to date. This conclusion is consistent with device photocurrent data indicating that the internal quantum efficiency (absorbed photon to electron quantum yield) for photocurrent generation in most DSSC devices is independent of excitation wavelength.[77] One study found that the reorganization energy (λ) for electron injection was small (~0.25 eV), and therefore would have only a minor impact on the injection rate.[69]

A more significant consideration for dye excited state energetics, and their impact upon electron injection, is the potential for injection from both the singlet and triplet excited states of the dye. This is particularly important for transition metal based dyes, such as ruthenium bipyridyl dyes, where the presence of a heavy metal center can result in intersystem crossing from the singlet to triplet excited states on ultrafast time scales (100 fs or faster) with a near unity quantum yield. A consideration of the triplet electron injection and its completion with excited state decay to ground is given in section 4.2 below.

The final term in eq 1 which should be considered in designing materials for fast electron injection is the electronic coupling term V. The magnitude of this coupling is primarily determined by the spatial overlap between the LUMO orbital of the dye excited state and the acceptor conduction band orbitals on the semiconductor. This wave function overlap is dependent both upon the distance of the dye LUMO orbital from the metal oxide surface, and the choice of anchoring group. Most studies suggest that through bond electron coupling, proceeding directly through anchor group and any spacer units if present, dominates over through space coupling. The most systematic studies of the influence of electronic coupling upon electron injection have employed dyes with nonconjugated spacer units between anchor group and chromophore, and have typically observed an exponential decrease in injection rate with increased spacer length (as illustrated in Figure 9).[116−125]

The position and nature of the anchoring group also plays a key role in determining the electronic coupling and therefore k_{inj}. For example, carboxylate anchoring groups have been shown to favor electron injection by allowing delocalization of the dye LUMO orbital over this anchoring group toward the metal oxide surface.[1,17,108,116,126−128] In addition, for ruthenium bipyridine dyes, carboxylates have been shown to favor electron injection by lowering the LUMO energy of the bipyridine unit attached to the carboxylates, thereby ensuring the dye LUMO orbital is localized upon the bipyridine unit closest to the metal oxide surface. For phthalocyanine based dyes we have found that axial out of plane anchoring groups showed poor injection rates[129] in comparison with peripheral anchoring ones; in the latter case the extension of the conjugation over the anchoring group is likely to play a key role. Recently Ooyama et al. reported a new type of D−π−A sensitizer dye employing intermolecular hydrogen bonding to increase the electron transfer rate.[130]

An interesting question is raised by the correlation of injection rates and efficiencies with the energy of the dye excited state relative to the measured exponential density of semiconductor acceptor states. The assumption made above is that the dyes inject into a continuum of states within this distribution. However, the states themselves are most often described as electron traps caused by a localized defect. Under this latter model, the 200 trap states per particle mentioned above, even if all on the surface, results in only one acceptor for every ~4 nm^2 of surface. Thus each dye would be in contact with at most 1 acceptor state, with a particular energy above or below the energy of the excited electron on the dye. In this sense the application of single, homogeneous calculation of electron transfer rate, such as eq 1, is questionable. If individual dyes are injecting into states with different energies, a range of injection times would result. This would be at least qualitatively consistent with experimental

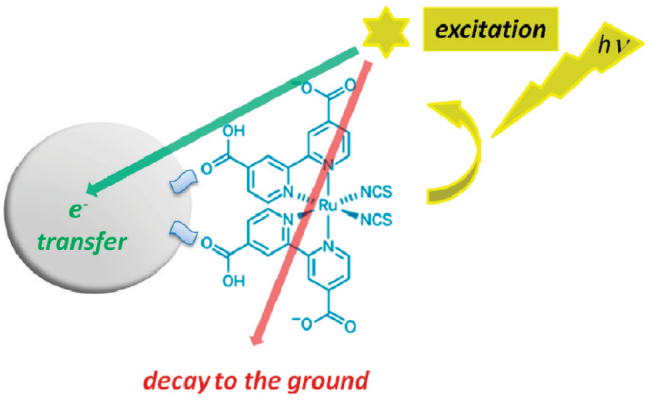

Figure 10. Schematic representation of the competition between electron injection and decay to the ground from the dye excited state.

observations that injection dynamics are typically characterized by stretched exponential rather than monoexponential kinetics.[15,76,77] Possible refinements to current considerations could include exciton migration along the dye layer, and/or a different view of surface "traps" that sees them as dynamic (in energy and position) surface states created by the TiO_2 surface interaction with the electrolyte and it is constituents. Lastly, the use of eq 1 implies a strong temperature dependence to the rate constant of injection. Temperature-independent injection rates have been observed in situations where fast injection into high density conduction band states should be relevant.[131] However, the temperature dependence of injection in optimized high efficiency cells has not been measured, to the best of our knowledge.

4.2. Excited State Decay to Ground. The quantum yield for electron injection, η_{inj}, corresponding to the fraction of photons absorbed by the dye that result in electron injection into the conduction band of TiO_2, is determined by

$$\eta_{inj} = \frac{k_{inj}}{k_{inj} + k_0 + k_q} \qquad (2)$$

where k_0 represents the rate constant for radiative and nonradiative decay of the excited state of isolated dye molecules, and k_q represents possible quenching pathways of the dye excited state in the device apart from electron injection (see Figure 10). Possible origins for k_q include dye aggregation resulting in an enhancement of nonradiative decay to ground[110,132−134] and reductive quenching of the dye excited state by oxidized redox couple.[135] k_0 and k_q can be most readily measured by employing metal oxides with a sufficiently high conduction band energy to prevent electron injection, such as mesoporous zirconia films.[15]

We have considered the factors determining k_{inj} in section 4.1 above. We now consider the competing path of excited state decay to ground, k_0. In this regard, the photoactive dyes employed for DSSCs can be broadly classified into two separate classes: inorganic coordination dyes which include a transition metal in the structure and organic dyes such as coumarins or porphyrins which do not include a heavy metal. Visible-light absorption in such organic dyes is typically based upon $\pi-\pi^*$ transitions to form singlet excited states. Intersystem crossing (ISC) to the lower energy triplet state is typically relatively slow (nanoseconds) and thus such dyes are primarily regarded as singlet sensitizers, with values of k_0 in the range 1×10^{10} to 1×10^8 s^{-1} (singlet excited state lifetimes ranging from ∼100 ps to a few nanoseconds). In contrast, for inorganic coordination dyes such as Ru-bipyridyls, the presence of the heavy metal center results in ultrafast intersystem crossing (<100 fs)[136] from the singlet to triplet excited state, with such dyes thus typically being regarded as triplet sensitizers, with values of k_0, corresponding to triplet state decay to ground, in the range 1×10^8 to 1×10^6 s^{-1} (triplet state lifetimes of tens to hundreds of nanoseconds).[77,114,137] This difference in dye photophysics has a significant impact upon the kinetics, energetics and efficiency of electron injection. This difference is illustrated in Figure 11 for a comparison of a typical organic dye **NKX2677** with the widely used Ru-bipyridyl dye, **N719**.

For the organic dye NKX2677, electron injection proceeds directly from the singlet excited state. This injection process is in competition with singlet state decay to ground (0.5 ns for this dye), requiring $k_{inj} > 2 \times 10^{10}$ s^{-1} to achieve an injection quantum yield of 90% or more. For the **N719** dye, electron injection may proceed from with the singlet or triplet excited state. The triplet state is ∼300 meV lower in energy than the singlet state, resulting, as discussed in section 4.1, in k_{inj} being exp(−300/100) ∼ 20-fold slower from the triplet compared to the singlet excited state. This difference in injection rates is consistent with previous reports of biphasic injection dynamics for **N3** sensitized TiO_2 films,[114,138] assigned to parallel pathways for electron injection from the **N3** singlet and triplet states. However, the slower electron injection from the **N719** triplet state is more than offset by a $\sim 1 \times 10^5$ increase in excited state lifetime, going from ∼100 fs for the singlet state to ∼10 ns for the triplet. As a consequence, electron injection from the triplet state of **N719** is likely to be more efficient than from the singlet state. Given the ∼10 ns lifetime of the **N719** triplet state, $k_{inj} \gtrsim 1 \times 10^9$ s^{-1} is sufficient to achieve an injection quantum yield of 90%.

We note that this argument does not preclude electron injection from the singlet excited state of **N719**. Indeed several studies have reported femtosecond injection kinetics for **N719** sensitized TiO_2 films.[69,117,138−140] However, such ultrafast electron injection is observed under conditions where the conduction band edge is energetically well below the dye excited state (such as in the presence of lithium ions), thereby increasing $\rho(E)$. Such conditions result in a large free energy loss associated with the injection and thermalization processes (in which the electrons thermalize to the CBE, and then to the TiO_2 Fermi level). The greater free energy loss associated with conditions giving ultrafast injection results in poor overall device efficiency, as discussed further in section 4.3 below. We further note that studies of triplet state driven electron injection have now been extended to other sensitizer dyes including ruthenium phthalocyanines, which exhibit long triplet state lifetimes such that reasonably efficient electron injection can be observed even on the 100s of nanoseconds time scale.[78,109]

We turn now to consideration of k_q, and specifically the effects of dye aggregation and quenching by the redox couple. The relatively planar structure of many organic dyes results in these dyes being relatively prone to aggregation, which often results in the enhancement of nonradiative decay pathways, thus reducing the efficiency of electron injection .[78,110,132−134] Commonly the incident photon-to-electron conversion efficiency (IPCE) in organic dye based devices are improved by addition of coadsorbers to break up dye aggregates.[110,141] In addition, the dye excited state can be quenched by the redox couple species present in the electrolyte.[108,135,142−145] The iodine based redox couple can

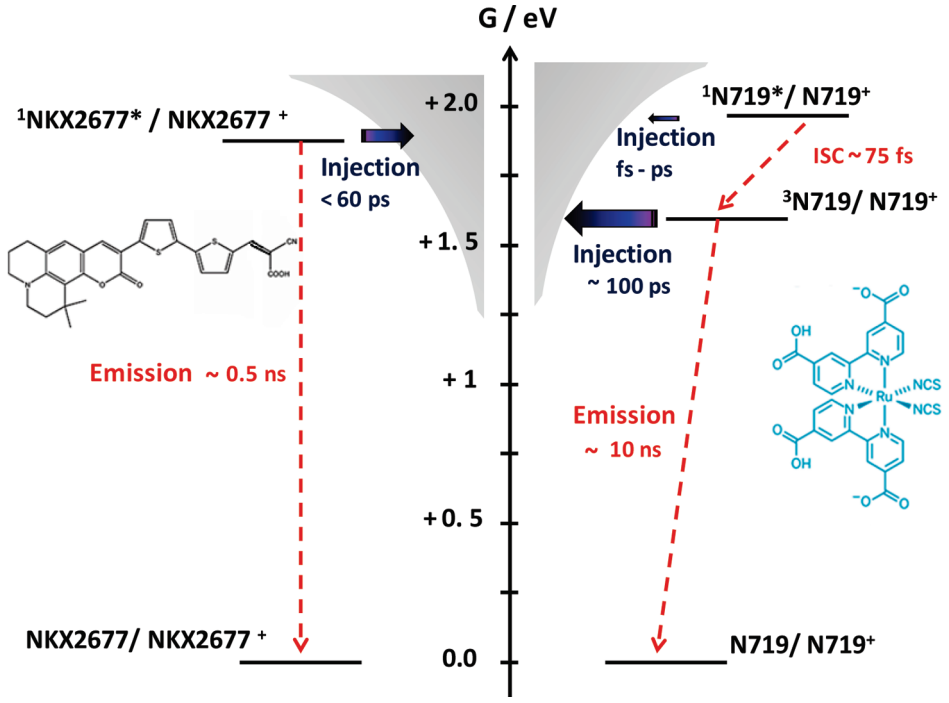

Figure 11. Illustration of the energetics and kinetics of electron injection for DSSCs based on a typical organic dye **NKX2677**, and the typical Ru-bipyridyl dye, **N719**. The TiO_2 acceptor states are shown as an exponential distribution in light gray. Energies are given as free energies relative to the dye ground state. Adapted with permission from ref 60. Copyright 1992 American Chemical Society.

quench the dye excited states by either oxidative or reductive quenching

$$\mathrm{Dye^*} + \mathrm{I_2} \rightarrow \mathrm{Dye^+} + \mathrm{I_2^-} \quad (3)$$

$$\mathrm{Dye^*} + \mathrm{I^-} \rightarrow \mathrm{Dye^-} + \frac{1}{2}\mathrm{I_2} \quad (4)$$

The presence of oxidative quenching (eq 3) will reduce the efficiency of charge separation, while reductive quenching (eq 4) may still result in efficient charge photogeneration if the dye anion is capable of efficiently injecting an electron into the semiconductor. The extent of these quenching pathways depends upon sensitizer dye and concentration of redox couple. For example, quenching of the dye excited state by the redox couple does not appear to be significant for the **N719** sensitizer dye, but has been observed for porphyrins.[108,146] Evidence for this quenching limiting photocurrent generation has been reported for devices employing a high concentration of redox couple, as sometimes used for high stability devices.[135] In solid state DSSCs, reductive quenching, in other words hole injection before electron injection has been reported in cells employing the molecular hole conductor spiro-OMeTAD, because of the strong electronic coupling between the sensitizer dye and hole conductor in these devices.[147,148] Picosecond hole injection into inorganic hole conductors has been observed for dye-sensitized CuSCN.[149]

4.3. Electron Injection in Complete DSSCs. Surprisingly few studies have considered directly the importance of electron injection in influencing DSSC photovoltaic efficiency. This absence can be understood as originating from the conclusions of early model systems studies on dye-sensitized TiO_2 films (including our own)[69,74,83,114,117,138−140,150,151] which indicated that electron injection from sensitizer dyes into metal oxides can occur on femtosecond time scales. This led to a widespread perception that electron injection in DSSC is always ultrafast, and therefore proceeds with near unity quantum efficiency. This perception has, however, become increasingly at variance with empirical device efficiency studies, which have shown that although photocurrent generation with near unity quantum efficiencies is possible for DSSCs with the appropriate choice of optimum materials, for many material choices, photocurrent quantum yields are significantly below unity. Increasingly it has become apparent that such lower photocurrent efficiencies may often originate from inefficient electron injection. In parallel, studies of electron injection in complete devices have indicated that injection dynamics in such devices may be significantly slower than in some model system studies, indeed resulting, for some devices, in electron injection efficiency being a significant limitation upon overall device efficiency.[15,77]

One of the first studies which provided clear evidence that injection efficiency may significantly limit photocurrent generation for some sensitizer dyes was undertaken by Hara et al., employing a series of organic sensitizer dyes.[93,110,111] In this study, the IPCE performance of DSSCs based on a series of coumarin dyes was found to correlate strongly with dye excited state oxidation potential, as shown in Figure 12. The reduction in maximal IPCE for dyes with less reducing excited states was assigned to lower charge separation yields resulting from less favorable energetics for electron injection.

Alternative studies have considered the impact of "potential determining ions" (see section 2.2) upon the energetics, and therefore efficiency, of electron injection. These include studies as a function of dye acidity,[75] and the presence of additives such as lithium ions and *tert*butylpyridine (tBP, a base) in the electrolyte.[60,65−69] Several such studies assigned the increase

in photocurrent with increased proton/lithium concentration to enhanced electron injection efficiency.[65−69] The first study which directly correlating electron injection dynamics measured in devices with device photocurrent efficiency was undertaken by Haque et al.[15] This study employed ultrafast transient absorption spectroscopy to show that injection dynamics in **N719** sensitized TiO_2 films was approximately 2 orders of magnitude slower in the presence of a typical redox electrolyte (∼100 ps), assigned to the influence of tBP in the electrolyte upon the energetics, and therefore kinetics of electron injection.

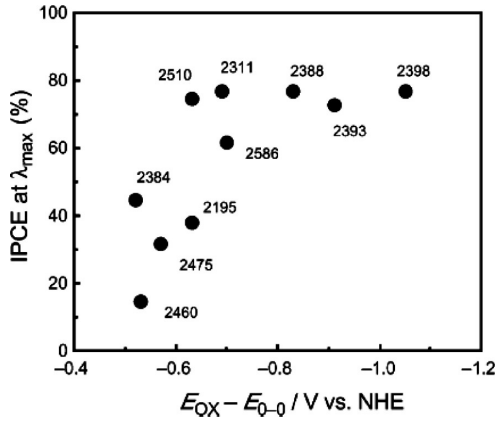

Figure 12. Maximal IPCE for DSSCs based on a series of coumarin dyes plotted as a function of dye excited state oxidation potential $E_{ox}^* = E_{ox} - E_{0-0}$. Reproduced with permission from ref 110.

Most recently, both we and others[77,78,147,152−155] have employed time correlated single photon counting to measure injection kinetics and yields in a range of DSSC, and correlated such measurements directly with device photocurrent. Such studies include studies as a function of lithium ions and tBP in the electrolyte (see Figure 13),[77,154] dye excited state oxidation potential and spacer conjugation.[108] In each case, a correlation was observed between the efficiency of electron injection, as determined by the transient kinetic data, and the photocurrent density measured under solar irradiation. These studies have been supported by analyses of front and back excitation IPCE data, which allow the separate determination of charge photogeneration and collection losses within devices, which have measured charge separation efficiencies in quantitative agreement with those determined by transient kinetic studies[156]

It follows from these analyses that the kinetics, and therefore efficiency, of electron injection are a function not only of the sensitizer dye and metal oxide, but also electrolyte composition. In general, for any given sensitizer/metal oxide combination, the kinetics of electron injection can be accelerated by increasing the concentration of potential determining ions in the electrolyte, up to the limits of ion solubility or dye desorption. The effect of increasing the concentration of these potential determining ions can be understood most simply as changing the surface charge of the metal oxide, resulting in interfacial dipoles which lowers the energetics of the metal oxide acceptor states $\rho(E)$ relative to the

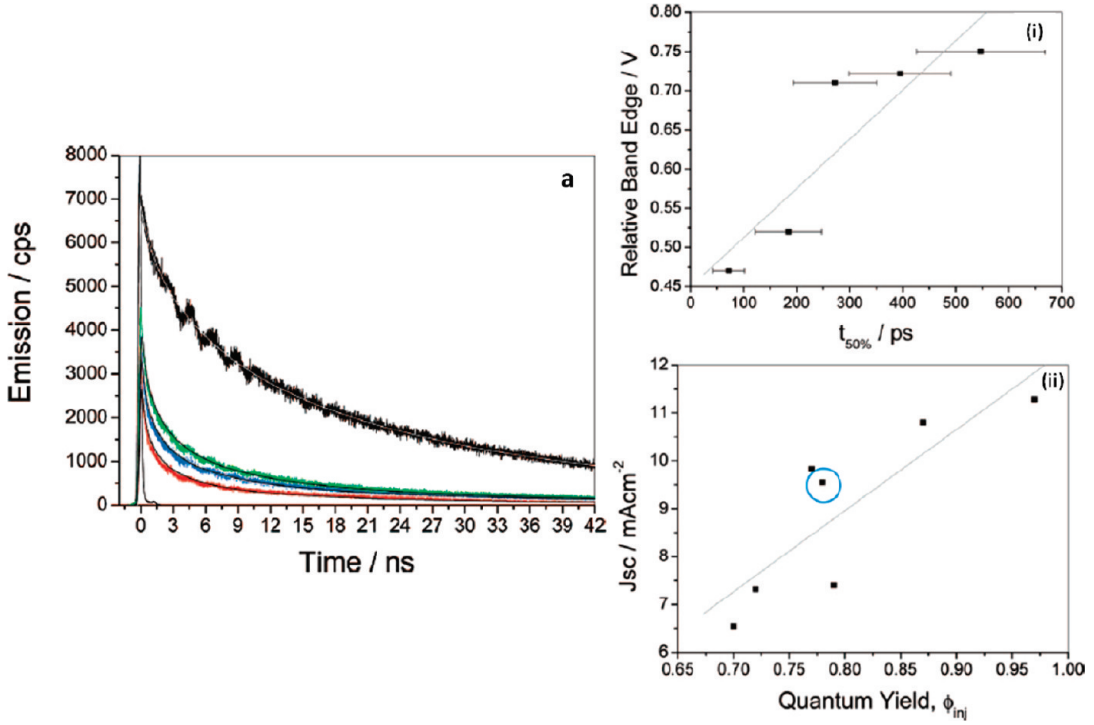

Figure 13. (a) Time-resolved emission decays for **N719**/TiO_2 films in electrolytes employing 0.1 M tBP/0.1 M Li^+ (red), 0.2 M tBP/0.1 M Li^+ (blue), and 0.2 M tBP/0 M Li^+ (green). Also shown are the corresponding **N719**/ZrO_2 control data (black) and (smooth lines) the fits to experimental data. (i) Plot of the electron injection half-time determined from TCSPC data versus an estimate of the relative energies of the TiO_2 CB determined from charge extraction data for DSSCs fabricated with different concentrations of Li^+ and tBP in the electrolyte. (ii) The corresponding plot of the electron injection yield, φ_{inj}, determined from TCSPC data versus the device short circuit currents measured under 1 sun simulated irradiation. Also shown are the linear best fits in gray. In (ii), the data point corresponding to the highest device efficiency is circled in blue. It is apparent that the device with the fastest injection dynamics, and highest injection yield, does not correspond to the device with the highest overall device efficiency. Reproduced with permission from ref 77.

dx.doi.org/10.1021/cm200651e |*Chem. Mater.* 2011, 23, 3381–3399

dye excited state oxidation potential E_{ox}* (and redox couple chemical potential) such as to increase the number of energetically accessible acceptor states. However it is important to note that this beneficial effect upon electron injection, and therefore device photocurrent, is often offset by a loss of cell voltage. The lower metal oxide conduction band energy results, for a given cell voltage or film Fermi level (see section 2.2), in a higher electron density in the metal oxide, thereby increasing the flux of interfacial recombination. Another way to view this balance between kinetics and energetics is that increasing the concentration of potential determining ions increases the kinetics of electron injection, but at the expense of a greater free energy loss associated with this injection process. More quantitively, following section 4.1 above, the energetic cost of increasing the rate of electron injection by 1 order of magnitude is ~300 meV. This concept has been discussed in terms of the need to minimize 'kinetic redundancy' in the device — with for example unnecessarily fast injection dynamics being indicative of an excessive free energy loss driving this reaction.[15] The key consequence of this balance is that, for any given combination of sensitizer and metal oxide, it is necessary to select a optimum electrolyte composition to achieve efficient electron injection while avoiding excessive V_{oc} loss, and thereby achieving maximal power output (current × volts) from the device.

We note that the analysis in the above paragraph most probably oversimplifies the role of the electrolyte in modulating the kinetics of electron injection in DSSC, with additional effects likely to originate from, for example, the passivation of surface states. Furthermore, there remains some controversy over experimental measurements of the injection kinetics in the presence of electrolyte, with some studies reporting subpicosecond injection dynamics even in the presence of a typical electrolyte.[145,157] In addition, we note that there are other strategies which can also be employed to modulate the balance between injection and recombination at the dye/metal oxide interface, and thereby to achieve the optimum balance of kinetics and energetics for maximal device performance. These include surface treatments such as the deposition of metal oxide layers (such as $TiCl_4$ treatments[158] or the deposition of Nb_2O_5,[159] Al_2O_3,[51,160] $CaCO_3$[161] or MgO,[162] layers) or the use of donor−acceptor charge transfer dyes such as **N719** where the dye LUMO orbital is localized adjacent to the metal oxide surface.

In general, we might also expect the cell voltage to affect directly the kinetics of electron injection. As the film Fermi level is raised, increasing the electron density in the film, the density of unoccupied acceptor states in the film decreases, which will in general reduce k_{inj}. This effect corresponds to the Fermi occupancy term $f(E, E_F)$ in eq 1, and could potentially limit the cell voltage. Model system studies employing a three electrode cell in the absence of a redox couple have indeed observed a modest retardation of k_{inj} with increase E_F, consistent with eq 1.[69] However a study of the kinetics of electron injection in a typical **N719** sensitized device as function of applied voltage reported only a small influence of voltage upon k_{inj} over the operating conditions of the device, indicating that in practice, the acceleration in recombination losses to the electrolyte with increasing Fermi level is a more severe limit upon cell voltage for most DSSCs studied to date.[77]

Overall, there appears to be increasing evidence that the kinetic competition between injection and excited state decay to ground can be a key factor modulating the efficiency of DSSCs. In this regard, the electronic coupling between the dye LUMO orbital and semiconductor acceptor states, the excited state oxidation potential, and the dye excited state lifetime are all important materials parameters which may influence device performance. Of these parameters, we note that dye excited state lifetime has received the least attention to date. In principle, the use of sensitizer dyes with longer excited state lifetimes should enable either the use of lower bandgap sensitizer dyes with lower energy excited states and/or a reduction in the concentration of acidic potential determining ions in the device, increasing cell voltage. Such strategies have the potential to significantly increase device performance, with kinetic analyses indicating that a 10-fold increase in excited state lifetime (and therefore a 10-fold decrease in the electron transfer rate constant required for efficient injection) potentially enabling a 300 meV shift dye absorption onset. However, to date, we are not aware of any studies that have directly correlated device performance with dye excited state lifetime.

5. SECONDARY CHARGE SEPARATION: DYE REGENERATION BY THE REDOX COUPLE

5.1. Dye Regeneration by Iodide. Following electron injection, the ground state of the sensitizer is regenerated by rereduction of oxidized dyes by the redox couple in the electrolyte. This secondary charge separation step increases the lifetime of the photogenerated charges, as illustrated in Figure 4. It furthermore enables diffusion of oxidized species to the counter electrode — completing the device electrical circuit. However the increase in charge separation lifetime resulting from this dye regeneration reaction comes at a significant energetic cost. For the most commonly studied dye/electrolyte combination, **N719** and the iodide/iodine redox couple, most estimates of the interfacial energetics indicate that ~600 meV are lost in driving this regeneration reaction.[6,10] This is the largest single free-energy loss in the device, and developing strategies to minimize this loss is a key challenge for achieving further advances in device efficiency.

Efficient dye regeneration requires the rate of rereduction of the photooxidized dye (D^+) by the redox couple to exceed that of charge recombination of injected electrons with D^+. This competing recombination pathway is considered in section 5.2. In this section, we focus on the kinetics and mechanism of dye regeneration by the most commonly used redox couple, iodine/iodide. Alternative redox couples, and molecular hole conductors, are considered in section 5.4.

Studies of the kinetics of the regeneration reaction have typically been based upon transient absorption studies of the decay of dye cation absorption, and/or the recovery of dye ground state absorption.[138,163,164] Typical data are shown in Figure 14. The detailed interpretation of these kinetics remains somewhat controversial, not least because of shifts in transient spectra caused by Stark effects generated by the electric field between the injected electrons and the electrolyte[81,165] Notwithstanding these uncertainties, several studies have indicated that in regeneration dynamics by iodide are typically on the microsecond time scale.

Various mechanisms have been proposed for the regeneration reaction. A major division between the reaction schemes is whether the reaction is first or second order in I^- concentration.[164,166,167] Several studies, including density functional theory (DFT) calculations,[168] have already led to a deeper understanding of the dye regeneration chemistry.[6,167,169−171] A key consideration is the

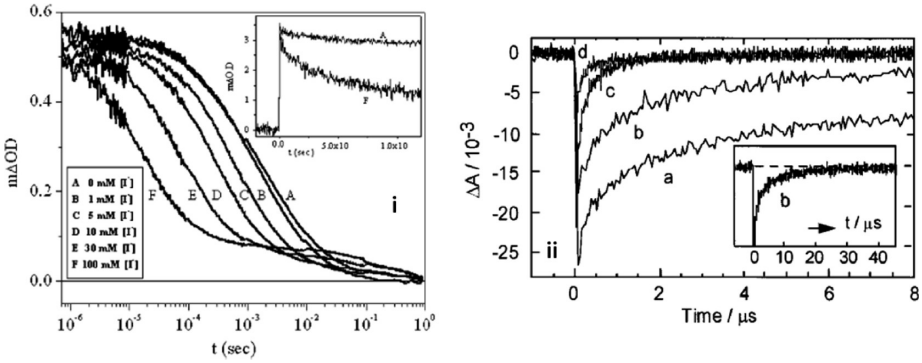

Figure 14. (i) Transient absorption data collected at 800 nm for a $Ru(dcbpy)_2(NCS)_2$-sensitized TiO_2 film measured as a function of iodide concentration. The electrolytes consisted of $LiClO_4$ and LiI in propylene carbonate, with the salt concentration adjusted to maintain a constant Li^+ concentration (0.1 M) while varying iodide concentrations as indicated in the figure. Also shown is an expansion of data collected at early times for I^- concentrations of 0 and 100 mM. Reproduced with permission from ref 163. Copyright 2002 American Chemical Society. (ii) Time course of the transient absorbance changes obtained upon nanosecond pulsed laser excitation (λ_{exc} = 490 nm, 5 ns fwhm pulse duration, 1 mJ/pulse) of $Ru(II)(dcbpy)_2(NCS)_2$ dye adsorbed on mesoporous TiO_2 films. Bleaching signals were measured at λ = 520 nm in dry propylene carbonate, without electrolyte (a), and in the presence of TBAI 0.1 M (b), LiI 0.1 M (c), and MgI_2 0.05 M (d). The insert displays trace (b) on a longer time scale. Reproduced with permission from ref 164. Copyright 2000 American Chemical Society.

unfavorable energetics for achieving the one electron oxidation of iodide to the iodine radical I·. As such, it has been widely suggested that the reaction proceeds through di-iodine radical ($I_2\cdot^-$), requiring the participation of two I^- for each oxidized dye (S^+).[6,169] Our own studies have provided evidence that the reaction can, at least for some sensitizer dyes, proceed via the formation of a oxidized dye − iodide complex. Transient absorption data suggest that formation of this complex is relatively rapid, with the rate determining step in the overall regeneration being the approach of a second I^- to this $[Dye^+...I^-]$ complex, releasing the products Dye and $I_2\cdot^-$.[172] At this point the regeneration is completed by the disproportionation of $I_2\cdot^-$. Consistent with this model, the overall regeneration reaction for the **N719** dye has been found to be first order in iodide.[169] Experimental measurements of the rate constant k_{rg} for this reaction have varied significantly in the literature,[163,164,166,173−175] with the most recent study reporting a value of $7.8 \times 10^5\ M^{-1}\ s^{-1}$ in methoxypropionitrile,[169] several orders of magnitude slower than the diffusion controlled rate constant in this solvent.

Several factors have been shown to influence the kinetics of regeneration. The most obvious is the dependence upon iodide concentration, as illustrated in Figure 14i.[163] In addition, the use of more viscous electrolytes (often used to reduce electrolyte volatility, and therefore enhance device stability) results in a retardation of regeneration.[36,37,41] The regeneration kinetics have also been reported to depend upon the identity of the cation of the iodide salt in the electrolyte; faster regeneration was observed in the presence of cations that adsorb onto the TiO_2 surface, such as Li^+ and Mg^{2+}, whereas much slower regeneration was found with TBA^+ ions, see Figure 14ii. This effect was attributed to the resulting higher local iodide concentration near the TiO_2 surface when positive charge is adsorbed.[164]

The design of the sensitizer also has a key role in influencing the kinetics of dye regeneration. For example, the addition of bulky alkyl chains to the dye has been found to slow the regeneration rate, assigned to the steric and nonpolar shielding effect offered to the metal oxidized center.[176] Other studies have considered the role of dye oxidation potential in influencing regeneration kinetics and efficiency, as discussed in section 5.3 below.

5.2. Electron Dye Recombination. In the absence of a redox active electrolyte, the oxidized dye is rereduced by charge recombination with electrons occupying conduction band or trap states of the metal oxide. The kinetics of recombination reaction have been widely reported to be superlinearly dependent upon electron density in these conduction band/trap states—resulting in the time scale of this recombination reaction ranging from nanoseconds to milliseconds, depending upon film electron Fermi level, and therefore electron density.[65,83,177−181] This strong dependence upon electron density has been discussed in the context of trap filling, with increased electron density resulting in the filling of the deepest electron traps, and therefore resulting in an increase in electron diffusion constant.[82,105,182−186] These traps may also act as recombination sites,[18,187−189] though as yet there is no conclusive evidence for this. The key implication of this electron density dependence for device performance is that the kinetics of this recombination reaction accelerate as the cell voltage is increased, and as light intensity increases. As such, the role of this recombination reaction in limiting regeneration efficiency depends strongly upon the device operating condition.

Aside from this dependence upon electron density, the kinetics of this recombination reaction depends upon the metal oxide and sensitizer dye employed, as illustrated in Figure 15 for two typical examples. For the sensitizer dye, the key factor is the spatial location of the dye cation HOMO orbital relative to the metal oxide surface. Localization of the HOMO orbital away from the metal oxide surface increases the electron tunneling barrier for recombination.[11,70,72,190,191] This has been shown most clearly for metal to ligand charge transfer dyes such as **N719**, where electron injection occurs from the π^* orbitals of a surface-bound dcb ligand, whereas recombination proceeds to the t_{2g} orbitals of the Ru(III)-$(NCS)_2$ center. It has also been reported that charge recombination is in the Marcus inverted region (see Figure 17 below), in contrast to electron injection, which has been reported to be nearly activationless.[83,72] Further studies have addressed "interface engineering" approaches to retard this interfacial charge recombination processes, including in particular the use of metal oxide barrier layers such as Nb_2O_5,[159] Al_2O_3,[51,160] $CaCO_3$,[161] and MgO.[162]

dx.doi.org/10.1021/cm200651e |*Chem. Mater.* 2011, 23, 3381–3399

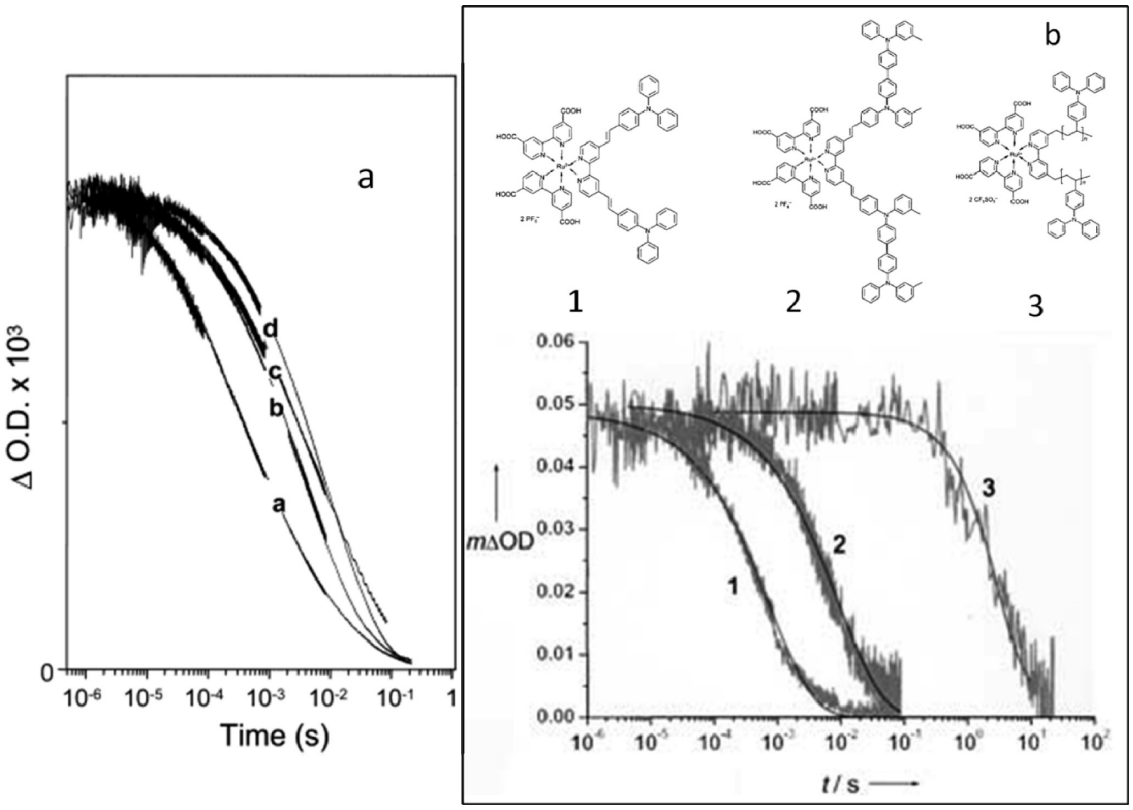

Figure 15. (a) Transient absorption data monitoring photoinduced absorption of the $RuL_2(NCS)_2$ cation following optical excitation of the dye adsorbed on nanoporous (a) TiO_2, (b) Al_2O_3/TiO_2, (c) SiO_2/TiO_2, and (d) ZrO_2/TiO_2 photoelectrodes. The signal decay is assigned to charge recombination of the dye cation with electrons in trap/conduction band states of the TiO_2 semiconductor. Optical excitation is at 630 nm, and detection at 800 nm. Reproduced with permission from ref 160. Copyright 2003 American Chemical Society. (b) Transient absorption data obtained for nanocrystalline TiO_2 films sensitized with dyes **1**−**3**. The decay kinetics are assigned to the charge recombination of the photogenerated dye cations with the electrons in the TiO_2. Reproduced with permission from ref 70. Copyright 2005 Wiley.

5.3. Role of Dye Regeneration in Limiting Device Performance. For DSSCs employing standard sensitizer dyes such as **N719** and relatively nonviscous electrolytes with high iodide concentrations, dye regeneration proceeds with near unity quantum yield. Indeed many device models have implicitly assumed recombination losses during regeneration to be negligible.[192] We emphasize that this high quantum efficiency comes a significant free energy cost, with the free energy loss driving regeneration ΔG_{rg} typically estimated at ~600 meV. However attention is now focusing on enhanced device longevity, typically involving the use of more viscous electrolytes, and lower bandgap sensitizer dyes, often reducing the free-energy driving regeneration. Both such strategies tend to result in slower regeneration kinetics, with therefore the potential for significant recombination losses during regeneration.

Alebbi and co-workers reported one of the first studies indicating that inefficient regeneration may limit device photocurrent.[173] This study focused upon a comparison of osmium and ruthenium based sensitizers. The osmium dye exhibited stronger near-infrared absorption, but a smaller ground state oxidation potential, reducing the driving force for the regeneration reaction, as illustrated in Figure 16. The lower photocurrents showed by the osmium based devices were assigned to slower iodide regeneration of the dye ground state.[173]

Several examples have now reported of dyes with less positive oxidation potentials showing slower regeneration.[148,172,173,193,194] These slower regeneration kinetics have in each case been

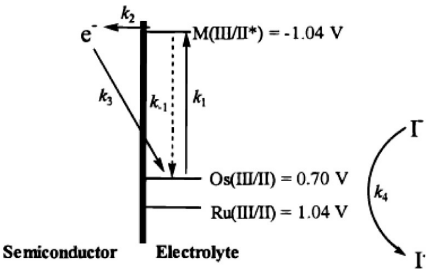

Figure 16. Energy level diagram for regeneration function in osmium and ruthenium dye sensitized solar cells. Reproduced with permission from ref 173.

suggested to result in increased quantum efficiency losses due to inefficient kinetic competition with electron recombination with dye cations, reducing device photocurrent. In contrast, rapid regeneration kinetics of the oxidized dye by iodide, with a high quantum efficiency, has been reported for sensitizers with comparatively high oxidation potentials, such as chlorophyll derivates[195] and porphyrins.[163] For a series of osmium and ruthenium complexes, a clear threshold behavior has been reported, with dyes exhibiting ΔG_{rg} < 600 mV for the iodide regeneration reaction not being effectively regenerated, see Figure 17.[72,73] A qualitatively similar trend between ΔG_{rg} and regeneration efficiency has been reported by Clifford et al. for a

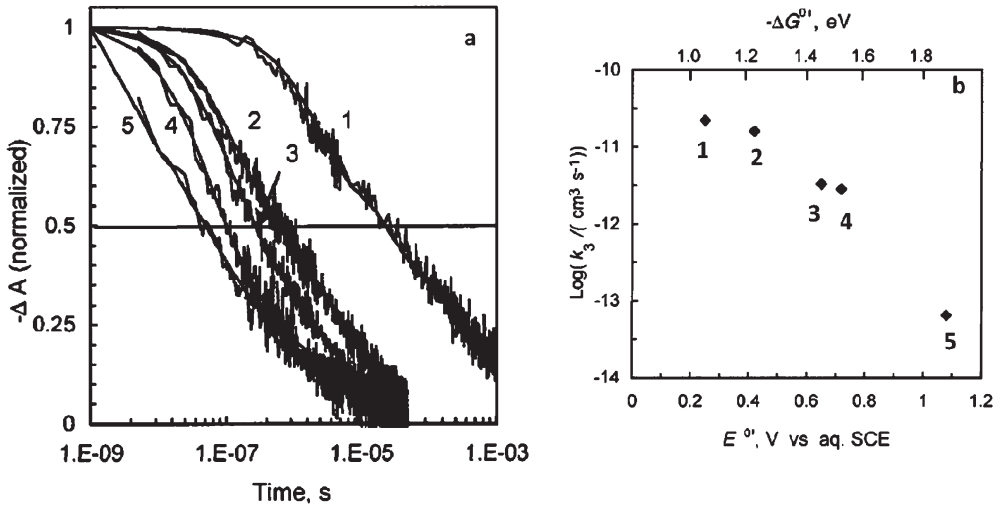

Figure 17. (a) Transient absorption kinetics measured for titanium dioxide photoelectrodes sensitized with different osmium and ruthenium polypyridyl complexes. The data were measured at 500 nm for complexes **1** $[Ru(H_2L')_2(CN)_2]$, **2** $[Os(H_2L')_2(CN)_2]$, and **5** $[Os(H_2L')_2Cl_2]$, and at 520 nm for complexes **3** $[Ru(H_2L')_2(NCS)_2]$ and **4** $[Os(H_2L')_2(NCS)_2]$. (b) Dependence of the recombination rate constant determined from the data shown in panel a upon the ground-state oxidation potential of complexes **1**-**5**. Also shown is the estimated driving force $-\Delta G^{o\prime}$ for the charge recombination process. Reproduced with permission from ref 72. Copyright 2001 American Chemical Society.

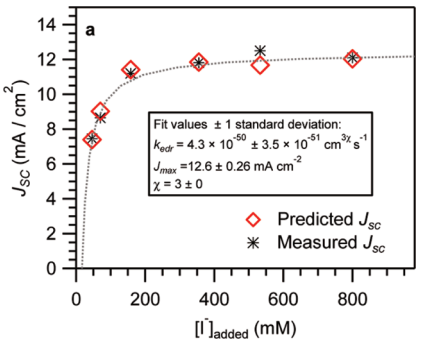

Figure 18. Measured and calculated J_{sc} for N719 sensitized DSSCs employing a methoxypropionitrile electrolyte The calculated J_{sc} were determined from measurements of the kinetics, and thereby the efficiency, of dye regeneration as a function of iodide concentration in a functioning device under operation.[196]

series of ruthenium-based dyes.[172] For osmium based DSSCs, it has been reported that the slower regeneration rate constant can be at least partly by offset by the use of higher I^- concentrations.[193]

We have recently reported an analysis of the kinetic competition between regeneration and recombination in **N719** sensitized devices under operation. The decrease in device photocurrent with lower iodide concentrations was found to be in good agreement with transient measurements of the regeneration quantum efficiency, as illustrated in Figure 18.[196]

A further consideration for such studies, particularly for higher viscosity electrolytes, is iodide depletion in the pores under operation.[196,197] The viscosity and the iodide content of the electrolyte are key issues for the technological scalability of such devices—high-performance electrolytes being typically less viscous and containing smaller concentrations of I^-, whereas higher stability electrolytes are typically more viscous and contain higher iodide concentrations. Higher iodide concentration reduces V_{oc} slightly (via the shift in the electrolyte redox potential), can further increase the viscosity of the electrolyte and, in the case of the imidazolium iodide salts, increases cost.

In addition to studies of the influence of regeneration upon device photocurrent, several studies have considered its impact upon cell fill factor and voltage.[36,198] In DSSCs, the down turn in photocurrent as the cell voltage is increased results from increasing electron concentration in the TiO_2.[10,197] At issue is the relative importance of recombination with the electrolyte versus that with the dye cation. Studies of this issues have to date largely focused upon polymer electrolytes,[36,198] where the lower iodide diffusion constant results in recombination losses during regeneration being particularly important.

5.4. Dye Regeneration by Alternative Redox Couples. The iodine couple is popular for DSSCs since it shows a slow rate of electron recombination with this electrolyte, fast diffusion, and an acceptable regeneration rate of the dye ground state at achievable concentrations. Nevertheless, there are substantial drawbacks to the use of the I_3^-/I^- couple as a redox shuttle in DSSCs.[6] These include: (i) a propensity to corrode non-noble metal components (this issue is important in the design of commercial DSSCs modules) (ii) limitations on the achievable open-circuit voltage (V_{oc}) due to the relatively negative redox potential of this shuttle, (iii) potential limitations on the achievable photocurrent due to the issue of using iodide to regenerate far-red-absorbing dyes at acceptable rates and (iv) limitations on the achievable photocurrent due to competitive absorption of visible light by triiodide. This latter is small in normal cells, but becomes significant in cells on metal substrates which are illuminated through the counter electrode. Clearly, it would be desirable to identify alternative, noncorrosive, and weakly absorbing redox reagents requiring lower energetic driving force for dye regeneration.[10] Br_2/Br^- and quinone/hydroquinone redox mediators were used with some success in early DSSC designs.[199] Pseudohalogen couples, $(SCN)_2/SCN^-$ and $(SeCN)_2/SeCN^-$, have also been employed.[200] Although redox potentials of these mediators are more positive than that of I_3^-/I^-, little improvement on the open circuit potential of the cells was observed.[200] Moreover, low power conversion efficiencies were obtained with

dx.doi.org/10.1021/cm200651e |Chem. Mater. 2011, 23, 3381–3399

these systems, which were attributed to slow dye regeneration reaction. A two electron redox couple based on 5-mercapto-1-methyltetrazole ions and its oxidized dimer have been tested recently reaching impressive overall conversion efficiencies of 6.4%[197] although some concerns exist regarding the stability of this class of mediator due to the radicals involved in the reaction.[201] Kinetically fast, one electron, couples, such as ferrocene/ferrocenium (Fc/Fc^+),[50,51,53] cobalt complexes (Co(II)/Co(III)),[52,202,203] copper complexes (Cu(I)/(II)),[48] and mediator mixtures,[49] have been used with some interesting results for DSSCs, despite the high rate of recombination with the electrons. In particular the last two years have seen a rapid increase in the reported efficiency of Fc and Co electrolytes which now look very promising.[202,204] Although it must be noted that little stability data has been presented for such new electrolytes, this is clearly an exciting research area which may significantly impact upon the commercial viability of DSSCs, as has been reviewed recently elsewhere.[205]

For alternative couples based on one electron reactions, such as Fc and Co electrolytes, the main issue is the fast recombination of the electrons traveling through the nanoparticles with oxidized species of the electrolyte. It is possible to reduce such recombination losses by the use of metal oxide barrier layers (see above) or by molecular/supramolecular insulating materials such as polymerized organic layers,[50,206,207] oligosaccharides,[208,209] and dendrimers.[210] Among the alternatives to iodine-based couples, cobalt complexes have reached the highest performances. These latter mediators have been thought to show deficient diffusive charge transport, due to the bulky dimension of these complexes.[52,203] However, by matching the properties of the dye and the cobalt redox mediator, Boshloo et al. were recently able to obtain an overall conversion efficiencies of 6.7%. This result was reached by reducing recombination through the introduction of insulating butoxyl chains on the dye and by reducing the thickness of the titania film thanks to the employment of a high extinction coefficient organic dye.[202]

Because of concerns over solvent leakage and corrosion, attention has also focused on replacing liquid electrolytes with solid state hole transporters to create fully solid state, electronic DSSCs. For this approach, spiro-MeOTAD has proven to be most successful, attributed to its acceptable charge carrier mobility, amorphous nature, and high solubility. Since the introduction of this approach, significant advances have been made, leading to device efficiencies for such solid-state DSSCs of up to ~5%, as has been discussed in detail elsewhere.[2,57,147,211]

6. CONCLUDING COMMENTS

This review has hopefully given the reader some insights into the parameters determining the efficiencies of electron injection and dye regeneration in dye sensitized photoelectrochemical solar cells. Enhancing the efficiency of DSSC is critically dependent upon maintaining near unity quantum efficiencies for these charge separation processes, while at the same time reducing the energetic losses required to drive these reactions. Addressing this challenge is fundamental to the challenges of enhancing the voltage output of devices, and of utilizing sensitizer dyes with lower optical bandgaps and therefore enhanced spectral overlap with the solar spectrum. A further challenge is to move toward materials which can achieve similar device performance but with enhanced stability and/or processability and lower cost. There is an increasing appreciation that meeting these challenges is a multidimensional problem, where any one materials change impacts upon several processes within the device. As such, systematic device optimization is increasingly dependent upon functional studies to guide materials design. We hope this review will prove to be useful resource for those addressing these key challenges for implementation of DSSCs as a commercially viable solar energy technology.

AUTHOR INFORMATION

Corresponding Author

*E-mail: j.durrant@imperial.ac.uk (J.R.D.); b.oregan@imperial.ac.uk (B.O.).

ACKNOWLEDGMENT

We gratefully acknowledge the many insightful discussions we have had with members of the DSSC research community, which have been instrumental in our arriving at the understanding summarized in this review. We also gratefully acknowledge financial support from the EU and EPSRC Supergen and APEX programmes.

REFERENCES

(1) O'Regan, B.; Gratzel, M. *Nature* **1991**, *353*, 737–740.
(2) Snaith, H. J.; Moule, A. J.; Klein, C.; Meerholz, K.; Friend, R. H.; Gratzel, M. *Nano Lett.* **2007**, *7*, 3372–3376.
(3) Durrant, J. R.; Gratzel, M. In *Nanostructured and Photoelectrochemical Systems for Solar Photon Conversion*; Archer, M. D., Nozik, A. J., Eds.; Imperial College Press: London, 2008.
(4) Mishra, A.; Fischer, M. K. R.; Bauerle, P. *Angew. Chem., Int. Ed.* **2009**, *48*, 2474–2499.
(5) Robertson, N. *Angew. Chem., Int. Ed.* **2006**, *45*, 2338–2345.
(6) Boschloo, G.; Hagfeldt, A. *Acc. Chem. Res.* **2009**, *42*, 1819–1826.
(7) Caramori, S.; Cristino, V.; Boaretto, R.; Argazzi, R.; Bignozzi, C. A.; Di Carlo, A. *Int. J. Photoenergy* **2010**, 458614.
(8) Ning, Z. J.; Fu, Y.; Tian, H. *Energy & Environmental Science* **2010**, *3*, 1170–1181.
(9) Gratzel, M. *Acc. Chem. Res.* **2009**, *42*, 1788–1798.
(10) O'Regan, B. C.; Durrant, J. R. *Acc. Chem. Res.* **2009**, *42*, 1799–1808.
(11) Ardo, S.; Meyer, G. J. *Chem. Soc. Rev.* **2009**, *38*, 115–164.
(12) Hagfeldt, A.; Boschloo, G.; Sun, L. C.; Kloo, L.; Pettersson, H. *Chem. Rev.* **2010**, *110*, 6595–6663.
(13) Clifford, J. N.; Martínez-Ferrero, E.; Viterisi, A.; Palomares, E. *Chem. Soc. Rev.* **2011**, *40*, 1635–1646.
(14) Durrant, J. R.; Haque, S. A.; Palomares, E. *Coord. Chem. Rev.* **2004**, *248*, 1247–1257.
(15) Haque, S. A.; Palomares, E.; Cho, B. M.; Green, A. N. M.; Hirata, N.; Klug, D. R.; Durrant, J. R. *J. Am. Chem. Soc.* **2005**, *127*, 3456–3462.
(16) Anderson, N. A.; Lian, T. Q. *Annu. Rev. Phys. Chem.* **2005**, *56*, 491–519.
(17) Anderson, N. A.; Lian, T. *Coord. Chem. Rev.* **2004**, *248*, 1231–1246.
(18) Bisquert, J.; Fabregat-Santiago, F.; Mora-Sero, I.; Garcia-Belmonte, G.; Barea, E. M.; Palomares, E. *Inorg. Chim. Acta* **2008**, *361*, 684–698.
(19) Peter, L. *Acc. Chem. Res.* **2009**, *42*, 1839–1847.
(20) Boschloo, G.; Haggman, L.; Hagfeldt, A. *J. Phys. Chem. B* **2006**, *110*, 13144–13150.
(21) Mori, S.; Sunahara, K.; Fukai, Y.; Kanzaki, T.; Wada, Y.; Yanagida, S. *J. Phys. Chem. C* **2008**, *112*, 20505–20509.
(22) van de Lagemaat, J.; Frank, A. J. *J. Phys. Chem. B* **2000**, *104*, 4292–4294.
(23) O'Regan, B. C.; Durrant, J. R.; Sommeling, P. M.; Bakker, N. J. *J. Phys. Chem. C* **2007**, *111*, 14001–14010.

(24) Snaith, H. J. *Adv. Funct. Mater.* **2010**, *20*, 13–19.
(25) Zhang, G. L.; Bala, H.; Cheng, Y. M.; Shi, D.; Lv, X. J.; Yu, Q. J.; Wang, P. *Chem. Commun.* **2009**, 2198–2200.
(26) Diamant, Y.; Chappel, S.; Chen, S. G.; Melamed, O.; Zaban, A. *Coord. Chem. Rev.* **2004**, *248*, 1271–1276.
(27) Zhang, Q. F.; Dandeneau, C. S.; Zhou, X. Y.; Cao, G. Z. *Adv. Mater.* **2009**, *21*, 4087–4108.
(28) Jose, R.; Thavasi, V.; Ramakrishna, S. *J. Am. Ceram. Soc.* **2009**, *92*, 289–301.
(29) Chen, S. G.; Chappel, S.; Diamant, Y.; Zaban, A. *Chem. Mater.* **2001**, *13*, 4629–4634.
(30) Tennakone, K.; Kumara, G.; Kottegoda, I. R. M.; Perera, V. P. S. *Chem. Commun.* **1999**, 15–16.
(31) Green, A. N. M.; Palomares, E.; Haque, S. A.; Kroon, J. M.; Durrant, J. R. *J. Phys. Chem. B* **2005**, *109*, 12525–12533.
(32) Kay, A.; Gratzel, M. *Chem. Mater.* **2002**, *14*, 2930–2935.
(33) Rensmo, H.; Keis, K.; Lindstrom, H.; Sodergren, S.; Solbrand, A.; Hagfeldt, A.; Lindquist, S. E.; Wang, L. N.; Muhammed, M. *J. Phys. Chem. B* **1997**, *101*, 2598–2601.
(34) Vayssieres, L.; Keis, K.; Hagfeldt, A.; Lindquist, S. E. *Chem. Mater.* **2001**, *13*, 4395–+.
(35) Zakeeruddin, S. M.; Gratzel, M. *Adv. Funct. Mater.* **2009**, *19*, 2187–2202.
(36) Upadhyaya, H. M.; Hirata, N.; Haque, S. A.; de Paoli, M. A.; Durrant, J. R. *Chem. Commun.* **2006**, 877–879.
(37) Haque, S. A.; Palomares, E.; Upadhyaya, H. M.; Otley, L.; Potter, R. J.; Holmes, A. B.; Durrant, J. R. *Chem. Commun.* **2003**, 3008–3009.
(38) Stathatos, E.; Chen, Y. J.; Dionysiou, D. D. *Sol. Energy Mater. Sol. Cells* **2008**, *92*, 1358–1365.
(39) Jovanovski, V.; Orel, B.; Jese, R.; Vuk, A. S.; Mali, G.; Hocevar, S. B.; Grdadolnik, J.; Stathatos, E.; Lianos, P. *J. Phys. Chem. B* **2005**, *109*, 14387–14395.
(40) Shi, D.; Pootrakulchote, N.; Li, R. Z.; Guo, J.; Wang, Y.; Zakeeruddin, S. M.; Gratzel, M.; Wang, P. *J. Phys. Chem. C* **2008**, *112*, 17046–17050.
(41) de Freitas, J. N.; Nogueira, A. F.; De Paoli, M. A. *J. Mater. Chem.* **2009**, *19*, 5279–5294.
(42) Durr, M.; Schmid, A.; Obermaier, M.; Rosselli, S.; Yasuda, A.; Nelles, G. *Nat. Mater.* **2005**, *4*, 607–611.
(43) Law, C. H.; Pathirana, S. C.; Li, X. O.; Anderson, A. Y.; Barnes, P. R. F.; Listorti, A.; Ghaddar, T. H.; O'Regan, B. C. *Adv. Mater.*, *22*, 4505-4509.
(44) Imahori, H.; Umeyama, T.; Ito, S. *Acc. Chem. Res.* **2009**, *42*, 1809–1818.
(45) Choi, H.; Raabe, I.; Kim, D.; Teocoli, F.; Kim, C.; Song, K.; Yum, J. H.; Ko, J.; Nazeeruddin, M. K.; Gratzel, M. *Chem.—Eur. J.* **2010**, *16*, 1193–1201.
(46) Hagberg, D. P.; Yum, J. H.; Lee, H.; De Angelis, F.; Marinado, T.; Karlsson, K. M.; Humphry-Baker, R.; Sun, L. C.; Hagfeldt, A.; Gratzel, M.; Nazeeruddin, M. K. *J. Am. Chem. Soc.* **2008**, *130*, 6259–6266.
(47) Ito, S.; Miura, H.; Uchida, S.; Takata, M.; Sumioka, K.; Liska, P.; Comte, P.; Pechy, P.; Graetzel, M. *Chem. Commun.* **2008**, 5194–5196.
(48) Brugnati, M.; Caramori, S.; Cazzanti, S.; Marchini, L.; Argazzi, R.; Bignozzi, C. A. *Int. J. Photoenergy* **2007**No. 80756.
(49) Cazzanti, S.; Caramori, S.; Argazzi, R.; Elliott, C. M.; Bignozzi, C. A. *J. Am. Chem. Soc.* **2006**, *128*, 9996–9997.
(50) Gregg, B. A.; Pichot, F.; Ferrere, S.; Fields, C. L. *J. Phys. Chem. B* **2001**, *105*, 1422–1429.
(51) Hamann, T. W.; Farha, O. K.; Hupp, J. T. *J. Phys. Chem. C* **2008**, *112*, 19756–19764.
(52) Nusbaumer, H.; Zakeeruddin, S. M.; Moser, J. E.; Gratzel, M. *Chem—Eur. J.* **2003**, *9*, 3756–3763.
(53) Feldt, S. M. ; U., B. C.; Johansson, E. M. J. ; Boschloo, G.; Hagfeldt, A. *J. Phys. Chem. C* **2010**, *114*, 10551–10558.
(54) Tennakone, K.; Kumara, G.; Kottegoda, I. R. M.; Wijayantha, K. G. U. *Semicond. Sci. Technol.* **1997**, *12*, 128–132.
(55) Oregan, B.; Schwartz, D. T. *J. Appl. Phys.* **1996**, *80*, 4749–4754.
(56) Bach, U.; Lupo, D.; Comte, P.; Moser, J. E.; Weissortel, F.; Salbeck, J.; Spreitzer, H.; Gratzel, M. *Nature* **1998**, *395*, 583–585.
(57) Wu, J. H.; Hao, S.; Lan, Z.; Lin, J. M.; Huang, M. L.; Huang, Y. F.; Li, P. J.; Yin, S.; Satot, T. *J. Am. Chem. Soc.* **2008**, *130*, 11568–+.
(58) Chiba, Y.; Islam, A.; Watanabe, Y.; Komiya, R.; Koide, N.; Han, L. Y. *Jpn. J. Appl. Phys., Part 2* **2006**, *45*, L638–L640.
(59) Lyon, L. A.; Hupp, J. T. *J. Phys. Chem. B* **1999**, *103*, 4623–4628.
(60) Rothenberger, G.; Fitzmaurice, D.; Gratzel, M. *J. Phys. Chem.* **1992**, *96*, 5983–5986.
(61) Redmond, G.; Okeeffe, A.; Burgess, C.; Machale, C.; Fitzmaurice, D. *J. Phys. Chem.* **1993**, *97*, 11081–11086.
(62) Nazeeruddin, M. K.; Humphry-Baker, R.; Liska, P.; Gratzel, M. *J. Phys. Chem. B* **2003**, *107*, 8981–8987.
(63) Zaban, A.; Ferrere, S.; Gregg, B. A. *J. Phys. Chem. B* **1998**, *102*, 452–460.
(64) O'Regan, B. C.; Bakker, K.; Kroeze, J.; Smit, H.; Sommeling, P.; Durrant, J. R. *J. Phys. Chem. B* **2006**, *110*, 17155–17160.
(65) Kelly, C. A.; Farzad, F.; Thompson, D. W.; Stipkala, J. M.; Meyer, G. J. *Langmuir* **1999**, *15*, 7047–7054.
(66) Asbury, J. B.; Anderson, N. A.; Hao, E. C.; Ai, X.; Lian, T. Q. *J. Phys. Chem. B* **2003**, *107*, 7376–7386.
(67) Park, N. G.; Chang, S. H.; van de Lagemaat, J.; Kim, K. J.; Frank, A. J. *Bulletin of the Korean Chemical Society* **2000**, *21*, 985–988.
(68) Watson, D. F.; Meyer, G. J. *Coord. Chem. Rev.* **2004**, *248*, 1391–1406.
(69) Tachibana, Y.; Haque, S. A.; Mercer, I. P.; Moser, J. E.; Klug, D. R.; Durrant, J. R. *J. Phys. Chem. B* **2001**, *105*, 7424–7431.
(70) Haque, S. A.; Handa, S.; Peter, K.; Palomares, E.; Thelakkat, M.; Durrant, J. R. *Angew. Chem., Int. Ed.* **2005**, *44*, 5740–5744.
(71) Barnes, P. R. F.; O'Regan, B. C. *J. Phys. Chem. C* **2010**, *114*, 19134–19140.
(72) Kuciauskas, D.; Freund, M. S.; Gray, H. B.; Winkler, J. R.; Lewis, N. S. *J. Phys. Chem. B* **2001**, *105*, 392–403.
(73) Kuciauskas, D.; Monat, J. E.; Villahermosa, R.; Gray, H. B.; Lewis, N. S.; McCusker, J. K. *J. Phys. Chem. B* **2002**, *106*, 9347–9358.
(74) Moser, J. E.; Gratzel, M. *Chimia* **1998**, *52*, 160–162.
(75) Tachibana, Y.; Nazeeruddin, M. K.; Gratzel, M.; Klug, D. R.; Durrant, J. R. *Chem. Phys.* **2002**, *285*, 127–132.
(76) Koops, S. E.; Durrant, J. R. *Inorg. Chim. Acta* **2008**, *361*, 663–670.
(77) Koops, S. E.; O'Regan, B. C.; Barnes, P. R. F.; Durrant, J. R. *J. Am. Chem. Soc.* **2009**, *131*, 4808–4818.
(78) Listorti, A.; López-Duarte, I.; Martínez-Díaz, M. V.; Torres, T.; DosSantos, T.; Barnes, P. R. F.; Durrant, J. R. *Energy Environ. Sci.* **2010**, accepted.
(79) Papageorgiou, N.; Athanassov, Y.; Armand, M.; Bonhote, P.; Pettersson, H.; Azam, A.; Gratzel, M. *J. Electrochem. Soc.* **1996**, *143*, 3099–3108.
(80) Barnes, P. R. F.; Anderson, A. Y.; Durrant, J. R.; O'Regan, B. C. *Phys. Chem. Chem. Phys.* **2011**, *13*, 5798–5816.
(81) Ardo, S.; Sun, Y.; Staniszewski, A.; Castellano, F. N.; Meyer, G. J. *J. Am. Chem. Soc.* **2010**, *132*, 6696–6709.
(82) Katoh, R.; Furube, A.; Barzykin, A. V.; Arakawa, H.; Tachiya, M. *Coord. Chem. Rev.* **2004**, *248*, 1195–1213.
(83) Moser, J. E.; Gratzel, M. *Chem. Phys.* **1993**, *176*, 493–500.
(84) Clarke, T. M.; Durrant, J. R. *Chem. Rev.* **2010**, *110*, 6736–6767.
(85) Gerischer, H.; Willig, F. *Top. Curr. Chem.* **1976**, *61*, 31–84.
(86) Gerischer, H. *Photochem. Photobiol.* **1972**, *16*, 243–260.
(87) Marcus, R. *J. Chem. Phys.* **1965**, *43*, 679–701.
(88) Prezhdo, O. V.; Duncant, W. R.; Prezhdo, V. V. *Acc. Chem. Res.* **2008**, *41*, 339–348.
(89) Gao, Y. Q.; Marcus, R. A. *J. Chem. Phys.* **2000**, *113*, 6351–6360.
(90) Cardon, F.; Gomes, W. P. *J. Phys. D: Appl. Phys.* **1978**, *11*, L63–L67.
(91) Westermark, K.; Henningsson, A.; Rensmo, H.; Sodergren, S.; Siegbahn, H.; Hagfeldt, A. *Chem. Phys.* **2002**, *285*, 157–165.
(92) Morris, A. J.; Meyer, G. J. *J. Phys. Chem. C* **2008**, *112*, 18224–18231.

(93) Hara, K.; Wang, Z. S.; Sato, T.; Furube, A.; Katoh, R.; Sugihara, H.; Dan-Oh, Y.; Kasada, C.; Shinpo, A.; Suga, S. *J. Phys. Chem. B* **2005**, *109*, 15476–15482.
(94) Katoh, R.; Furube, A.; Murai, M.; Tamaki, Y.; Hara, K.; Tachiya, M. *C. R. Chim.* **2006**, *9*, 639–644.
(95) Rehm, J. M.; McLendon, G. L.; Nagasawa, Y.; Yoshihara, K.; Moser, J.; Gratzel, M. *J. Phys. Chem.* **1996**, *100*, 9577–9578.
(96) Villanueva, J.; Anta, J. A.; Guillen, E.; Oskam, G. *J. Phys. Chem. C* **2009**, *113*, 19722–19731.
(97) Peter, L. M.; Walker, A. B.; Boschloo, G.; Hagfeldt, A. *J. Phys. Chem. B* **2006**, *110*, 13694–13699.
(98) Quintana, M.; Edvinsson, T.; Hagfeldt, A.; Boschloo, G. *J. Phys. Chem. C* **2007**, *111*, 1035–1041.
(99) Lee, J. J.; Coia, G. M.; Lewis, N. S. *J. Phys. Chem. B* **2004**, *108*, 5282–5293.
(100) Bailes, M.; Cameron, P. J.; Lobato, K.; Peter, L. M. *J. Phys. Chem. B* **2005**, *109*, 15429–15435.
(101) Duffy, N. W.; Peter, L. M.; Rajapakse, R. M. G.; Wijayantha, K. G. U. *Electrochem. Commun.* **2000**, *2*, 658–662.
(102) We note that electrochemical studies may be limited at high electron densities by band unpinning and accumulation layers, whilst XPS and related studies appear to be limited by the reorganization of the TiO_2 surface under vacuum which seems to form a large band of states ~1 eV below the conduction band.
(103) Schwanitz, K.; Weiler, U.; Hunger, R.; Mayer, T.; Jaegermann, W. *J. Phys. Chem. C* **2007**, *111*, 849–854.
(104) Nelson, J. *Phys. Rev. B* **1999**, *59*, 15374–15380.
(105) Nelson, J.; Haque, S. A.; Klug, D. R.; Durrant, J. R. *Phys. Rev. B: Condens. Matter Mater. Phys.* **2001**, 63.
(106) She, C. X.; Anderson, N. A.; Guo, L. C.; Chen, D. T.; Mohler, D.; Liu, F.; Hupp, J. T.; Lian, T. Q. *Abstr. Pap. Am. Chem. Soc.* **2005**, *230*, 316-PHYS.
(107) She, C. X.; Guo, J. C.; Lian, T. Q. *J. Phys. Chem. B* **2007**, *111*, 6903–6912.
(108) Dos Santos, T.; Morandeira, A.; Koops, S.; Mozer, A. J.; Tsekouras, G.; Dong, Y.; Wagner, P.; Wallace, G.; Earles, J. C.; Gordon, K. C.; Officer, D.; Durrant, J. R. *J. Phys. Chem. C* **2010**, *114*, 3276–3279.
(109) Morandeira, A.; LÃ³pez-Duarte, I.; MartÃ-nez-DÃ-az, M. V.; O'Regan, B.; Shuttle, C.; Haji-Zainulabidin, N. A.; Torres, T. s.; Palomares, E.; Durrant, J. R. *J. Am. Chem. Soc.* **2007**, *129*, 9250–9251.
(110) Hara, K.; Sato, T.; Katoh, R.; Furube, A.; Ohga, Y.; Shinpo, A.; Suga, S.; Sayama, K.; Sugihara, H.; Arakawa, H. *J. Phys. Chem. B* **2003**, *107*, 597–606.
(111) Zhang, X.; Zhang, J. J.; Xia, Y. Y. *J. Photochem. Photobiol., A: Chem.* **2008**, *194*, 167–172.
(112) Koops, S. E.; Barnes, P. R. F.; O'Regan, B. C.; Durrant, J. R. *J. Phys. Chem. C* **2010**, *114*, 8054–8061.
(113) Benko, G. b.; Kallioinen, J.; Korppi-Tommola, J. E. I.; Yartsev, A. P.; Sundstrom, V. *J. Am. Chem. Soc.* **2001**, *124*, 489–493.
(114) Kallioinen, J.; Benko, G.; Sundstrom, V.; Korppi-Tommola, J. E. I.; Yartsev, A. P. *J. Phys. Chem. B* **2002**, *106*, 4396–4404.
(115) Bruggemann, B.; Organero, J. A.; Pascher, T.; Pullerits, T.; Yartsev, A. *Phys. Rev. Lett.* **2006**, 97.
(116) Heimer, T. A.; Darcangelis, S. T.; Farzad, F.; Stipkala, J. M.; Meyer, G. J. *Inorg. Chem.* **1996**, *35*, 5319–5324.
(117) Asbury, J. B.; Hao, E.; Wang, Y. Q.; Ghosh, H. N.; Lian, T. Q. *J. Phys. Chem. B* **2001**, *105*, 4545–4557.
(118) Smalley, J. F.; Feldberg, S. W.; Chidsey, C. E. D.; Linford, M. R.; Newton, M. D.; Liu, Y. P. *J. Phys. Chem.* **1995**, *99*, 13141–13149.
(119) Sikes, H. D.; Smalley, J. F.; Dudek, S. P.; Cook, A. R.; Newton, M. D.; Chidsey, C. E. D.; Feldberg, S. W. *Science* **2001**, *291*, 1519–1523.
(120) Creager, S.; Yu, C. J.; Bamdad, C.; O'Connor, S.; MacLean, T.; Lam, E.; Chong, Y.; Olsen, G. T.; Luo, J. Y.; Gozin, M.; Kayyem, J. F. J. Am. Chem. Soc. **1999**, *121*, 1059–1064.
(121) Houamer-Rassin, C.; Chaignon, F.; She, C.; Stockwell, D.; Blart, E.; Buvat, P.; Lian, T.; Odobel, F. *J. Photochem. Photobiol., A: Chem.* **2007**, *192*, 56–65.
(122) Anderson, N. A.; Ai, X.; Chen, D. T.; Mohler, D. L.; Lian, T. Q. *J. Phys. Chem. B* **2003**, *107*, 14231–14239.
(123) Asbury, J. B.; Hao, E. C.; Wang, Y. Q.; Lian, T. Q. *J. Phys. Chem. B* **2000**, *104*, 11957–11964.
(124) Piotrowiak, P.; Galoppini, E.; Wei, Q.; Meyer, G. J.; Wiewior, R. *J. Am. Chem. Soc.* **2003**, *125*, 5278–5279.
(125) Myahkostupov, M.; Piotrowiak, P.; Wang, D.; Galoppini, E. *J. Phys. Chem. C* **2007**, *111*, 2827–2829.
(126) Gillaizeau-Gauthier, I.; Odobel, F.; Alebbi, M.; Argazzi, R.; Costa, E.; Bignozzi, C. A.; Qu, P.; Meyer, G. J. *Inorg. Chem.* **2001**, *40*, 6073–6079.
(127) Odobel, F.; Blart, E.; Lagree, M.; Villieras, M.; Boujtita, H.; El Murr, N.; Caramori, S.; Bignozzi, C. A. *J. Mater. Chem.* **2003**, *13*, 502–510.
(128) She, C. X.; Guo, J. C.; Irle, S.; Morokuma, K.; Mohler, D. L.; Zabri, H.; Odobel, F.; Youm, K. T.; Liu, F.; Hupp, J. T.; Lian, T. *J. Phys. Chem. A* **2007**, *111*, 6832–6842.
(129) Palomares, E.; Martinez-Diaz, M. V.; Haque, S. A.; Torres, T.; Durrant, J. R. *Chem. Commun.* **2004**, 2112–2113.
(130) Ooyama, Y.; Inoue, S.; Asada, R.; Ito, G.; Kushimoto, K.; Komaguchi, K.; Imae, I.; Harima, Y. *Eur. J. Org. Chem.* **2010**, 92–100.
(131) Burfeindt, B.; Hannappel, T.; Storck, W.; Willig, F. *J. Phys. Chem.* **1996**, *100*, 16463–16465.
(132) Wenger, B.; Gratzel, M.; Moser, J. E. *J. Am. Chem. Soc.* **2005**, *127*, 12150–12151.
(133) Zanotti, G.; Angelini, N.; Notarantonio, S.; Paoletti, A. M.; Pennesi, G.; Rossi, G.; Lembo, A.; Colonna, D.; Di Carlo, A.; Reale, A.; Brown, T. M.; Calogero, G. *Int. J. Photoenergy* **2010**No. 268035.
(134) Lu, H. P.; Tsai, C. Y.; Yen, W. N.; Hsieh, C. P.; Lee, C. W.; Yeh, C. Y.; Diau, E. W. G. *J. Phys. Chem. C* **2009**, *113*, 20990–20997.
(135) Wang, P.; Wenger, B.; Humphry-Baker, R.; Moser, J. E.; Teuscher, J.; Kantlehner, W.; Mezger, J.; Stoyanov, E. V.; Zakeeruddin, S. M.; Gratzel, M. *J. Am. Chem. Soc.* **2005**, *127*, 6850–6856.
(136) Damrauer, N. H.; Cerullo, G.; Yeh, A.; Boussie, T. R.; Shank, C. V.; McCusker, J. K. *Science* **1997**, *275*, 54–57.
(137) Juris, A.; Balzani, V.; Barigelletti, F.; Campagna, S.; Belser, P.; Vonzelewsky, A. *Coord. Chem. Rev.* **1988**, *84*, 85–277.
(138) Tachibana, Y.; Moser, J. E.; Gratzel, M.; Klug, D. R.; Durrant, J. R. *J. Phys. Chem.* **1996**, *100*, 20056–20062.
(139) Asbury, J. B.; Ellingson, R. J.; Ghosh, H. N.; Ferrere, S.; Nozik, A. J.; Lian, T. Q. *J. Phys. Chem. B* **1999**, *103*, 3110–3119.
(140) Ellingson, R. J.; Asbury, J. B.; Ferrere, S.; Ghosh, H. N.; Sprague, J. R.; Lian, T. Q.; Nozik, A. J. *J. Phys. Chem. B* **1998**, *102*, 6455–6458.
(141) Zhang, X. H.; Li, C.; Wang, W. B.; Cheng, X. X.; Wang, X. S.; Zhang, B. W. *J. Mater. Chem.* **2007**, *17*, 642–649.
(142) Bergeron, B. V.; Meyer, G. J. *J. Phys. Chem. B* **2003**, *107*, 245–254.
(143) Clark, C. C.; Marton, A.; Srinivasan, R.; Sarjeant, A. A. N.; Meyer, G. J. *Inorg. Chem.* **2006**, *45*, 4728–4734.
(144) Marton, A.; Clark, C. C.; Srinivasan, R.; Freundlich, R. E.; Sarjeant, A. A. N.; Meyer, G. J. *Inorg. Chem.* **2006**, *45*, 362–369.
(145) Smeigh, A. L.; Katz, J. E.; Brunschwig, B. S.; Lewis, N. S.; McCusker, J. K. *J. Phys. Chem. C* **2008**, *112*, 12065–12068.
(146) Splan, K. E.; Massari, A. M.; Hupp, J. T. *J. Phys. Chem. B* **2004**, *108*, 4111–4115.
(147) Snaith, H. J.; Petrozza, A.; Ito, S.; Miura, H.; Gratzel, M. *Adv. Funct. Mater.* **2009**, *19*, 1810–1818.
(148) Tatay, S.; Haque, S. A.; O'Regan, B.; Durrant, J. R.; Verhees, W. J. H.; Kroon, J. M.; Vidal-Ferran, A.; Gavina, P.; Palomares, E. *J. Mater. Chem.* **2007**, *17*, 3037–3044.
(149) Oregan, B.; Schwartz, D. T. *Chem. Mater.* **1995**, *7*, 1349–1354.
(150) Pelet, S.; Gratzel, M.; Moser, J. E. *J. Phys. Chem. B* **2003**, *107*, 3215–3224.
(151) Ghosh, H. N.; Asbury, J. B.; Lian, T. Q. *J. Phys. Chem. B* **1998**, *102*, 6482–6486.
(152) Reynal, A.; Forneli, A.; Palomares, E. *Energy Environ. Sci.* **2010**, *3*, 805–812.
(153) Cid, J. J.; Garcia-Iglesias, M.; Yum, J. H.; Forneli, A.; Albero, J.; Martinez-Ferrero, E.; Vazquez, P.; Gratzel, M.; Nazeeruddin, M. K.; Palomares, E.; Torres, T. *Chem—Eur. J.* **2009**, *15*, 5130–5137.

(154) Planells, M.; Cespedes-Guirao, F. J.; Goncalves, L.; Sastre-Santos, A.; Fernandez-Lazaro, F.; Palomares, E. *J. Mater. Chem.* **2009**, *19*, 5818–5825.
(155) Werner, F.; Gnichwitz, J. F.; Marczak, R.; Palomares, E.; Peukert, W.; Hirsch, A.; Guldi, D. M. *J. Phys. Chem. B* **2010**, *114*, 14671–14678.
(156) Barnes, P. R. F.; Liu, L. X.; Li, X. E.; Anderson, A. Y.; Kisserwan, H.; Ghaddar, T. H.; Durrant, J. R.; O'Regan, B. C. *Nano Lett.* **2009**, *9*, 3532–3538.
(157) Kuang, D. B.; Ito, S.; Wenger, B.; Klein, C.; Moser, J. E.; Humphry-Baker, R.; Zakeeruddin, S. M.; Gratzel, M. *J. Am. Chem. Soc.* **2006**, *128*, 4146–4154.
(158) Sommeling, P. M.; O'Regan, B. C.; Haswell, R. R.; Smit, H. J. P.; Bakker, N. J.; Smits, J. J. T.; Kroon, J. M.; van Roosmalen, J. A. M. *J. Phys. Chem. B* **2006**, *110*, 19191–19197.
(159) Zaban, A.; Chen, S. G.; Chappel, S.; Gregg, B. A. *Chem. Commun.* **2000**, 2231–2232.
(160) Palomares, E.; Clifford, J. N.; Haque, S. A.; Lutz, T.; Durrant, J. R. *J. Am. Chem. Soc.* **2003**, *125*, 475–482.
(161) Okada, N.; Karuppuchamy, S.; Kurihara, M. *Chem. Lett.* **2005**, *34*, 16–17.
(162) Grinis, L.; Kotlyar, S.; Ruhle, S.; Grinblat, J.; Zaban, A. *Adv. Funct. Mater.* **2010**, *20*, 282–288.
(163) Montanari, I.; Nelson, J.; Durrant, J. R. *J. Phys. Chem. B* **2002**, *106*, 12203–12210.
(164) Pelet, S.; Moser, J. E.; Gratzel, M. *J. Phys. Chem. B* **2000**, *104*, 1791–1795.
(165) Cappel, U. B.; Feldt, S. M.; Schoneboom, J.; Hagfeldt, A.; Boschloo, G. *J. Am. Chem. Soc.* **2010**, *132*, 9096–9101.
(166) Fitzmaurice, D. J.; Frei, H. *Langmuir* **1991**, *7*, 1129–1137.
(167) Gardner, J. M.; Giaimuccio, J. M.; Meyer, G. J. *J. Am. Chem. Soc.* **2008**, *130*, 17252–+.
(168) Privalov, T.; Boschloo, G.; Hagfeldt, A.; Svensson, P. H.; Kloo, L. *J. Phys. Chem. C* **2009**, *113*, 783–790.
(169) Anderson, A. Y.; Barnes, P. R. F.; Durrant, J. R.; O'Regan, B. C. *J. Phys. Chem. C* **2010**, *114*, 1953–1958.
(170) Schiffmann, F.; VandeVondele, J.; Hutter, J.; Urakawa, A.; Wirz, R.; Baiker, A. *Proc. Natl. Acad. Sci. U.S.A.* **2010**, *107*, 4830–4833.
(171) Gardner, J. M.; Abrahamsson, M.; Farnum, B. H.; Meyer, G. J. *J. Am. Chem. Soc.* **2009**, *131*, 16206–16214.
(172) Clifford, J. N.; Palomares, E.; Nazeeruddin, M. K.; Gratzel, M.; Durrant, J. R. *J. Phys. Chem. C* **2007**, *111*, 6561–6567.
(173) Alebbi, M.; Bignozzi, C. A.; Heimer, T. A.; Hasselmann, G. M.; Meyer, G. J. *J. Phys. Chem. B* **1998**, *102*, 7577–7581.
(174) Nasr, C.; Hotchandani, S.; Kamat, P. V. *J. Phys. Chem. B* **1998**, *102*, 4944–4951.
(175) Heimer, T. A.; Heilweil, E. J.; Bignozzi, C. A.; Meyer, G. J. *J. Phys. Chem. A* **2000**, *104*, 4256–4262.
(176) Kroeze, J. E.; Hirata, N.; Koops, S.; Nazeeruddin, M. K.; Schmidt-Mende, L.; Gratzel, M.; Durrant, J. R. *J. Am. Chem. Soc.* **2006**, *128*, 16376–16383.
(177) Oregan, B.; Moser, J.; Anderson, M.; Gratzel, M. *J. Phys. Chem.* **1990**, *94*, 8720–8726.
(178) Hasselmann, G. M.; Meyer, G. J. *J. Phys. Chem. B* **1999**, *103*, 7671–7675.
(179) Haque, S. A.; Tachibana, Y.; Willis, R. L.; Moser, J. E.; Gratzel, M.; Klug, D. R.; Durrant, J. R. *J. Phys. Chem. B* **2000**, *104*, 538–547.
(180) Haque, S. A.; Tachibana, Y.; Klug, D. R.; Durrant, J. R. *J. Phys. Chem. B* **1998**, *102*, 1745–1749.
(181) Martini, I.; Hodak, J. H.; Hartland, G. V. *J. Phys. Chem. B* **1999**, *103*, 9104–9111.
(182) Nelson, J.; Kirkpatrick, J.; Ravirajan, P. *Phys. Rev. B: Condens. Matter Mater. Phys.* **2004**, 69.
(183) Gaal, D. A.; Hupp, J. T. *J. Am. Chem. Soc.* **2000**, *122*, 10956–10963.
(184) Gaal, D. A.; Hupp, J. T. *Semicond. Photochem. Photophys.* **2003**, *10*, 89–121.
(185) Barzykin, A. V.; Tachiya, M. *J. Phys. Chem. B* **2002**, *106*, 4356–4363.
(186) Barzykin, A. V.; Tachiya, M. *J. Phys. Chem. B* **2004**, *108*, 8385–8389.
(187) Kavan, L.; Kratochvilova, K.; Gratzel, M. *J. Electroanal. Chem.* **1995**, *394*, 93–102.
(188) Boschloo, G.; Fitzmaurice, D. *J. Phys. Chem. B* **1999**, *103*, 2228–2231.
(189) Wang, H. L.; He, J. J.; Boschloo, G.; Lindstrom, H.; Hagfeldt, A.; Lindquist, S. E. *J. Phys. Chem. B* **2001**, *105*, 2529–2533.
(190) Clifford, J. N.; Palomares, E.; Nazeeruddin, M. K.; GrÃ¤tzel, M.; Nelson, J.; Li, X.; Long, N. J.; Durrant, J. R. *J. Am. Chem. Soc.* **2004**, *126*, 5225–5233.
(191) Kleverlaan, C.; Alebbi, M.; Argazzi, R.; Bignozzi, C. A.; Hasselmann, G. M.; Meyer, G. J. *Inorg. Chem.* **2000**, *39*, 1342–1343.
(192) Bisquert, J.; Mora-Sero, I. *J. Phys. Chem. Lett.* **2010**, *1*, 450–456.
(193) Onicha, A. C.; Castellano, F. N. *J. Phys. Chem. C* **2010**, *114*, 6831–6840.
(194) Li, X. Y.; Long, N. J.; Clifford, J. N.; Campbell, C. J.; Durrant, J. R. *New J. Chem.* **2002**, *26*, 1076–1080.
(195) Kay, A.; Humphry-Baker, R.; Graetzel, M. *J. Phys. Chem.* **1994**, *98*, 952–959.
(196) Anderson, A. Y.; Barnes, P. R. F.; Durrant, J. R.; O'Regan, B. C. *J. Phys. Chem. C* **2011**, *115*, 2439–2447.
(197) Barnes, P. R. F.; Anderson, Y. A.; Mindaugas, J.; Lingxuan, L.; Xiaoe, L.; Palomares, E.; Fornelli, A.; O'Regan, B. C. *Phys. Chem. Chem. Phys.* **2011**, *13*, 3547–3558.
(198) Nogueira, A. F.; De Paoli, M. A.; Montanari, I.; Monkhouse, R.; Nelson, J.; Durrant, J. R. *J. Phys. Chem. B* **2001**, *105*, 7517–7524.
(199) Desilvestro, J.; Gratzel, M.; Kavan, L.; Moser, J.; Augustynski, J. *J. Am. Chem. Soc.* **1985**, *107*, 2988–2990.
(200) Oskam, G.; Bergeron, B. V.; Meyer, G. J.; Searson, P. C. *J. Phys. Chem. B* **2001**, *105*, 6867–6873.
(201) Wang, M. K.; Chamberland, N.; Breau, L.; Moser, J. E.; Humphry-Baker, R.; Marsan, B.; Zakeeruddin, S. M.; Gratzel, M. *Nat. Chem.* **2010**, *2*, 385–389.
(202) Feldt, S. M.; Gibson, E. A.; Gabrielsson, E.; Sun, L.; Boschloo, G.; Hagfeldt, A. *J. Am. Chem. Soc.* **2010**, *132*, 16714–16724.
(203) Nusbaumer, H.; Moser, J. E.; Zakeeruddin, S. M.; Nazeeruddin, M. K.; Gratzel, M. *J. Phys. Chem. B* **2001**, *105*, 10461–10464.
(204) Daeneke, T.; Kwon, T.-H.; Holmes, A. B.; Duffy, N. W.; Bach, U.; Spiccia, L. *Nat. Chem.* **2011**, *3*, 213–217.
(205) Hamann, T. W.; Ondersma, J. W. *Energy Environ. Sci.* **2011**, *4*, 370–381.
(206) Lee, W.; Roh, S. J.; Hyung, K. H.; Park, J.; Lee, S. H.; Han, S. H. *Solar Energy* **2009**, *83*, 690–695.
(207) Pesek, J. J.; Matyska, M. T. *Interface Sci.* **1997**, *5*, 103–117.
(208) Handa, S.; Haque, S. A.; Durrant, J. R. *Adv. Funct. Mater.* **2007**, *17*, 2878–2883.
(209) Choi, H.; Kang, S. O.; Ko, J.; Gao, G.; Kang, H. S.; Kang, M. S.; Nazeeruddin, M. K.; Gratzel, M. *Angew. Chem., Int. Ed.* **2009**, *48*, 5938–5941.
(210) Satoh, N.; Nakashima, T.; Yamamoto, K. *J. Am. Chem. Soc.* **2005**, *127*, 13030–13038.
(211) Snaith, H. J.; Humphry-Baker, R.; Chen, P.; Cesar, I.; Zakeeruddin, S. M.; Gratzel, M. *Nanotechnology* **2008**, *19*, 424003.